Tryptophan-mediated Dimerization of the TssL Transmembrane Anchor Is Required for Type VI Secretion System Activity

Abdelrahim Zoued, Jean-Pierre Duneau, Eric Durand, Alexandre España, Laure Journet, Françoise Guerlesquin, E. Cascales

Tryptophan-mediated dimerization of the TssL transmembrane anchor is required for Type VI secretion system activity

Abdelrahim Zoued[†], Jean-Pierre Duneau*, Eric Durand, Alexandre P. España[§], Laure Journet, Françoise Guerlesquin* , and Eric Cascales*

Running title: Dimerization of the TssL transmembrane helix

Laboratoire d'Ingénierie des Systèmes Macromoléculaires (LISM), Institut de Microbiologie de la Méditerranée (IMM), Aix-Marseille Université, CNRS, UMR 7255, 31 chemin Joseph Aiguier, 13402 Marseille Cedex 20, France

[†] Current address: Howard Hughes Medical Institute, Brigham and Women's Hospital, Division of Infectious Diseases and Harvard Medical School, Department of Microbiology and Immunobiology, Boston, Massachusetts, USA.

[§] Current address: Technological Advances for Genomics and Clinics laboratory (TAGC, U1090), Aix-Marseille Univ. - Institut National de la Santé et de la Recherche Médicale (INSERM), 163 Avenue de Luminy, 13288 Marseille Cedex 09, France.

* To whom correspondence should be addressed:
Jean-Pierre Duneau (duneau@imm.cnrs.fr)
Françoise Guerlesquin (guerlesq@imm.cnrs.fr)
Eric Cascales (cascales@imm.cnrs.fr)

Abstract

The Type VI secretion system (T6SS) is a multiprotein complex used by bacteria to deliver effectors into target cells. The T6SS comprises a bacteriophage-like contractile tail structure anchored to the cell envelope by a membrane complex constituted of the TssJ outer membrane lipoprotein and the TssL and TssM inner membrane proteins. TssJ establishes contact with the periplasmic domain of TssM whereas the transmembrane segments of TssM and its cytoplasmic domain interact with TssL. TssL protrudes in the cytoplasm but is anchored by a C-terminal transmembrane helix (TMH). Here, we show that TssL TMH dimerization is required for the stability of the protein and for T6SS function. Using the TOXCAT assay and point mutations of the 23 residues of the TssL TMH we identified Thr194 and Trp199 as necessary for TssL TMH dimerization. NMR hydrogen-deuterium exchange experiments demonstrated the existence of a dimer with the presence of Trp185 and Trp199 at the interface. A structural model based on molecular dynamics simulations shows that TssL TMH dimer formation involves π-π interactions resulting from the packing of the two Trp199 rings at the C-terminus and of the six aromatic rings of Tyr184, Trp185 and Trp188 at the N-terminus of the TMH.

Introduction

The Type VI secretion system (T6SS) is a molecular machine widely distributed in proteobacteria and responsible for the contact-dependent secretion of effector proteins into target cells [1,2]. Effectors delivered by this apparatus interfere with eukaryotic host cell physiology, or cause damages in bacterial cells [3-6]. The T6SS is therefore involved in pathogenesis and/or bacterial competition. At the molecular level, the T6SS could be represented as a nano-speargun [7-9] (Fig. 1A): an inner tube made of stacked Hcp hexameric rings capped by the VgrG spike complex and wrapped by a contractile sheath is propelled into the target cells during sheath contraction [10-12]. This tubular structure is assembled on a sub-membrane platform – or baseplate – that comprises the TssEFGK and VgrG subunits and is anchored to the cell envelope by the membrane complex [13-18].

In enteroaggregagtive *Escherichia coli* (EAEC), the T6SS membrane core complex is constituted of the outer membrane-associated TssJ lipoprotein and the TssL and TssM inner membrane proteins [14,19,20] (Fig. 1B and C). TssJ folds as a classical transthyretin with an additional α-helix and an extended loop connecting β-strands 1 and 2 (L1-2) [21-23]. TssM comprises three transmembrane helices (TMH): TMH1 and TMH2 forms a hairpin located close to the N-terminus, separated from the third helix, TMH3, by a 35-kDa cytoplasmic domain [16,24] (Fig. 1C). The TssM cytoplasmic portion comprises two subdomains with structural homologies to NTPases and the DPY-30 dimerization hairpin [16]. The TssM cytoplasmic domain makes contact with TssL, as well as with TssG and TssK, two components of the tail assembly platform [13,15,16,18]. The majority of the EAEC TssM subunit (750 amino-acids) is located in the periplasm and its C-terminal extremity interacts with the TssJ lipoprotein L1-2 loop [14,21]. The EAEC TssL protein is a C-tail membrane protein, anchored to the inner membrane by a C-terminal TMH that requires the YidC

insertase for its insertion [25,26] (Fig. 1C). The TssL cytoplasmic domain comprises two 3-helix bundles [27-29] and interacts with two subunits of the baseplate, TssE and TssK [15,17]. In EAEC, this domain forms weak dimers, but the full-length protein (*i.e.*, comprising the C-terminal transmembrane anchor) is a stable dimer that resists Sodium Dodecyl Sulphate-Poly Acrylamide Gel Electrophoresis (SDS-PAGE; [27]).

The TssJLM membrane complex is the first T6SS structure to be assembled. Its biogenesis starts with the positioning of the TssJ lipoprotein and proceeds with the sequential addition of TssM and TssL [14]. Polymerization of this hetero-trimer requires local remodelling of the cell wall layer that is assured by a dedicated peptidoglycan hydrolase or a housekeeping transglycosylase [30,31]. Ten copies of the hetero-trimer polymerize to form the 5-fold symmetry transenvelope channel. The 12-Å negative-stain electron microscopy structure of the TssJLM complex from enteroaggregative *E. coli* has been reported [14] (Fig. 1B). It comprises a large base constituted of the cytoplasmic domains and transmembrane segments and a cap composed of TssJ. Base and cap are connected by pillars made of the TssM periplasmic domains [14]. The TssJLM structure has been obtained in a closed conformation and molecular dynamics (MD) simulations have suggested that large conformational modifications of the pillars cause opening of the structure for the passage of the inner tube during sheath contraction [14]. To resist the strength generated during sheath contraction, the TssJLM membrane complex is stably anchored to the cell wall by a peptidoglycan-binding domain either fused at the C-terminus of TssL or carried by an accessory component [20,32].

Although the EM structure of the EAEC TssJLM complex and the X-ray structures of the soluble domains of TssL, TssM and TssJ have been reported, little is known on the transmembrane portion of the complex. It has been shown that the C-terminal anchor of TssL is required for T6SS function and for stable dimerization of TssL [27]. We therefore sought to

gain insights into the structure of the TssL TMH and its dimerization determinants. TOXCAT analyses demonstrated that the TssL TMH is necessary and sufficient for dimerization. Functional assays further showed that TMH-mediated TssL dimerization is required for TssL stability and T6SS function. Finally, scanning site-directed mutagenesis coupled to TOXCAT, structural Nuclear Magnetic Resonance (NMR) studies and MD simulations defined that tryptophan rings engage in π-π interactions to mediate $TssL^{TM}$ dimerization.

Results

The TssL transmembrane segment is sufficient for dimerization.

Structure-function analyses of the T6SS TssL cytoplasmic domain revealed that it weakly dimerizes [17,27]). By contrast, the full-length protein forms dimers that are stable in SDS-PAGE [27]. We concluded that the C-terminal transmembrane helix strongly contributes to TssL dimerization. To test this hypothesis, we used the TOXCAT assay [33], a two-hybrid assay based on the reconstitution of an active ToxR dimeric regulator upon association of two transmembrane helices. The dimeric ToxR regulator binds the *tox* promoter and activates the expression of the gene encoding chloramphenicol acetyl-transferase and conferring resistance to chloramphenicol [33,34]. The sequence corresponding to the transmembrane helix of TssL ($TssL^{TM}$) was inserted between the ToxR' domain and the maltose-binding protein (MBP) to yield the ToxR'-$TssL^{TM}$-MBP fusion protein. Controls include the transmembrane helix of the glycophorin A (GpA), considered as a model for transmembrane helix association, as well as a point mutant disrupting dimerization of GpA (GpA^{G83I}) [33]. Cells producing ToxR'-$TssL^{TM}$-MBP grew on minimal medium with maltose as carbon source (Fig. 2A-B), demonstrating that the MBP localizes in the periplasm and hence that the construct is properly inserted in the membrane via the TssL transmembrane helix. Chloramphenicol disk and

chloramphenicol acetyl-transferase activity (Fig. 2C and 2D) assays further showed that TssL^{TM} dimerizes at levels comparable to the GpA control. From these data, we conclude that TssL^{TM} dimerizes by itself in the membrane.

Thr194 and Trp199 contribute to TssL^{TM} dimerization.

To get further information on the driving forces that control TssL^{TM} dimer formation, we used the same TOXCAT approach coupled to site directed mutagenesis screening. A number of motifs involved in transmembrane helix interactions have been reported, such as leucine zipper and GxxGxxxG motifs. Analyses of the TssL^{TM} sequence reveals the presence of a leucine zipper motif (LxxLxxxL) comprising Leu195, Leu198 and Leu202 (shown in red in Fig. 3A). Leucine zippers are common protein-protein interaction motifs, and such a motif has been shown to be involved in the dimerization of the T4SS-associated VirB10 transmembrane segment [35]. We first engineered mutations to break the TssL^{TM} leucine zipper motif by substituting Leu195 and Leu198 by alanines (LALA variant). TOXCAT assays show that mutations of these two leucine residues had only a slight effect on the ability of TssL^{TM} to dimerize (Fig. 3B and 3D) and thus contradict the leucine zipper hypothesis. To identify the residues of TssL^{TM} involved in dimer formation, we performed a systematic scanning mutagenesis, in which each individual residue has been changed to tryptophan. Tryptophan side-chains are bulky and have been previously shown to disrupt contacts between tightly packed transmembrane segments [36]. Tryptophan residues of TssL^{TM} were substituted by alanines. TOXCAT assays demonstrated that while a number of substitutions affect the stability of the TssL^{TM} dimer, only two mutations – Thr194Trp (T194W) and Trp199Ala (W199A) — have a level of chloramphenicol acetyl transferase activity comparable to the absence of TMH (Fig. 3C and 3D).

Previous data have shown that the TssL transmembrane helix stabilizes the TssL dimer, which then resists SDS-PAGE analysis [27]. We hence tested whether the T194W and W199A substitutions impact the stability of the TssL dimer in SDS-PAGE. As previously observed, the cytoplasmic domain of TssL ($TssL_C$) migrates as a monomer upon SDS-PAGE whereas the dimer of the full-length TssL protein is detected (Fig. 4, lanes 1 and 2 respectively). For the T194W and W199A variants of TssL only monomers are observed indicating that the T194W and W199A mutations have a strong effect on $TssL^{TM}$ dimer formation (Fig. 4, lanes 3 and 4).

Structural analysis of the $TssL^{TM}$ dimer interface

To investigate the structure of the $TssL^{TM}$ dimer, we first conducted Nuclear Magnetic Resonance (NMR) experiments using a synthetic peptide corresponding to the TssL transmembrane segment (Met183-Ala207), stabilized by two additional lysine residues at the N- and C-termini. The $TssL^{TM}$ peptide was solubilized in presence of SDS because (i) the $TssL^{TM}$ dimer has been shown to be stable in SDS-PAGE [27], (ii) in such context, SDS micelles have been previously shown to mimick the membrane environment [37], and (iii) SDS is commonly used for solution NMR analyses of transmembrane domains [38-40]. Proton assignment of the $TssL^{TM}$ peptide was obtained using TOCSY and NOESY data (Table S1). On the basis of NH/NH nuclear Overhauser effect restraint measurements we concluded that the sequential NH/NH distances are in agreement with a structure of the peptide as an extended α-helix (Fig. 5A, Fig. S1) [41]. The presence of a unique set of peaks in the NMR spectra suggested that the TssL peptide forms a symmetric dimer in SDS. In this case, it is quite impossible to distinguish intra and intermolecular distance restraints (nOes) at the interface using homonuclear NMR. To investigate the dimer interface, we used hydrogen-deuterium (H-D) exchange experiments by recording NOESY experiments in D_2O buffer. In

D_2O the NH groups exposed to the solvent are rapidly converted in ND groups that are not observed in the proton NMR spectra. By contrast, in these conditions, the NH groups protected by a hydrogen bond or by any other contact are slowly converted in ND groups and are still observed in the proton NMR spectra. Fig. 5B and 5C show that the Trp185 and Trp199 ring NHs are significantly more protected to the solvent exchange compared to the amide groups of the rest of the $TssL^{TM}$ peptide, likely because of their location at the dimer interface. Thus, the H-D exchange experiments support the conclusion of the TOXCAT assay that $TssL^{TM}$ dimer interface involves the Trp199 rings at the periplasmic side of the TMH and in addition, provides support to the location of the Trp185 rings at the interface at the cytoplasmic side of the TMH (Fig. 5D). However, rapid H-D exchange was observed for the amide group of Thr194, suggesting that it is not protected and thus that Thr194 is not located at the dimer interface. However, although the NMR approach demonstrated that $TssL^{TM}$ has an helical structure and is organized as a dimer in SDS with Trp185 and Trp199 at the interface, it was not possible to define the structure of $TssL^{TM}$ using classical approaches of homonuclear NMR.

Toward the aim to obtain a structural model of the $TssL^{TM}$ dimer and to better define the dimerization interface, we used molecular dynamics (MD) simulations. For comparison, these MD simulations were conducted in conditions identical to the NMR experiments (at 300K, in SDS micelle). First, a 50-ns simulation of the monomer peptide was performed in a SDS micelle containing 110 detergent molecules to generate the basic element, *i.e.*, the $TssL^{TM}$ monomer. Consistent with the NMR data, the averaged structure demonstrated that the $TssL^{TM}$ monomer is a straight α-helix in SDS environment (Fig. 5E and 6A). This structure further shows that Trp199 and Trp185 belong to the same helix face (Fig. 5E). By contrast, Thr194 and Trp199 belong to opposite faces (Fig. 5E and 6A), and hence, it is unlikely that both residues participate to a homodimeric interaction without substantial structure

disturbance. To explore if such distortions could arise in the context of the dimeric structure, we performed MD simulations of TssL^{TM} in the SDS micelle (*i.e.*, in conditions similar to the NMR and SDS-PAGE experiments, in which the TssL^{TM} dimer was observed). Starting from eight different symmetric conformations (see methods), the superimposition of the eight averaged structures (Fig. 6A) shows no significant changes of the structure of TssL^{TM}. Fig. 6B and 6C capture the proximity between the Thr194 or Trp199 in each dimer during the course of the 8 simulations (numbered from 0° to 350° according to the relative orientation of the helix faces). Interestingly, only the 250° simulation allows a tight proximity between the Thr194 of the two monomers (Fig. 6B), whereas the 0°, 50° and 350° simulations bring the Trp199 of both monomers at close proximity (Fig. 6C). These simulations also indicate that the Trp199 of one monomer is never close to the Thr194 residue of the other monomer. As suggested by the organization of residues on the face of the straight α-helix (Fig. 5E), the positioning of Trp199 at the interface also bring aromatic residues of the TssL^{TM} N-terminal region (Tyr184, Trp185, Trp188) in close proximity. To further address the role of the aromatic residues at the interface, the '0' and 350° simulations were prolonged for 100 ns (Fig. 6D and 6E). The two simulations converged to a very similar structure in which eight aromatic rings (Tyr184, Trp185, Trp188, Trp199 from each monomer) interact at the interface of the TMH dimer (Fig. 5F). Interestingly, Trp185 was protected in NMR H-D exchange experiments and thus described as an interfacial residue. Hence, modeling of the TssL^{TM} dimer confirms that (i) Thr194 and Trp199 are not located on the same interface, and (ii) that Trp199 likely contributes, as well as residues Tyr184, Trp185 and Trp188, to TssL^{TM} dimerization (Fig. 5F). The implication of Trp199 to TssL^{TM} dimerization during MD simulations validates the results of the TOXCAT assay and NMR H-D exchange experiments. By contrast to the TOXCAT assay, the NMR and MD data did not highlight a role for residue Thr194. To test whether the replacement of Thr194 by a Trp residue interfere with TssL^{TM}

dimerization, we performed MD simulations using the TssL^{TM} peptide bearing a Trp at position 194 (Fig. S2). This substitution significantly affects the contact map calculated for the TssL^{TM} dimer during a 50-ns simulation. Notably, the contacts that initially involved the N-terminal aromatic cluster decrease (see for example Trp188) to the advantage of new contacts that are formed on the C-terminal region of the peptide (Fig. S2A). From the initial position (in red), this drift leads to a more open conformation (in blue) that moves forward the two N-terminal extremities (Fig. S2B). This structural change corresponds to a huge rise in the root-mean square deviation (rmsd) of monomer B relative to monomer A, that reaches a plateau at ~5-6 Å in less than 5 ns, increasing to 10 Å after 20 ns, a behavior typical of a loss of structural stability (Fig. S2C). Hence, the lack of interaction between TssL^{TM} T194W variants in the TOXCAT assay might be correlated to a significant impairment of the TssL^{TM} dimer integrity that could arise from subtle conformational or dynamic alterations.

Transmembrane-mediated TssL dimerization is required for T6SS function.

The T6SS assembles a tail-like structure comprising the tail tube made of Hcp hexameric rings wrapped by the sheath. Contraction of the sheath is proposed to propel the Hcp tube toward the target cell. The presence of the Hcp protein in the culture supernatant is therefore a reporter of T6SS activity [42]. Indeed, Hcp is detected in the culture supernatant of a wild-type strain, whereas is absent in the culture supernatant of a Δ*tssL* mutant strain (Fig. 7A). The production of a plasmid-borne full-length TssL protein restores the release of Hcp. By contrast, despite the observation that the W199A variant is produced at levels comparable to wild-type TssL, this mutation abolishes Hcp release (Fig. 7A). The EAEC T6SS has anti-bacterial activity and has been shown to provide a competitive advantage against *E. coli* K-12 cells [43]. The results of the competition assays showed that cells producing the W199A TssL mutant are unable to eliminate competitor *E. coli* K-12 cells (Fig. 7B).

Taken together, the Hcp release and anti-bacterial competition assays demonstrate that the TssL W199A mutation prevents proper function of the Type VI secretion apparatus in EAEC, suggesting that T6SS function requires dimerization of the TssL transmembrane anchor.

TssL dimerization increases TssL stability.

To gain further insights onto the role of $TssL^{TM}$ dimerization during T6SS assembly, we tested whether disrupting $TssL^{TM}$ dimer formation impact the stability of the full-length TssL. EAEC cells producing TssL or TssL-W199A were subjected to protein synthesis arrest using the ribosomal 30S-specific spectinomycin antibiotic, and steady-state TssL levels were monitored over time. Fig. 8 shows that TssL is a rather stable protein with a half-life of ~ 50 min. The W199A substitution causes an important decrease of TssL stability, with a measured half-time < 10 min.

Ligand-induced dimerization of TssL

Our *in vivo* results, monitored in the context of the fully assembled T6SS, cannot exclude that the W199A substitution affects other functions or interactions in addition to $TssL^{TM}$ dimerization. We hence engineered TssL variants in which the genetically modified FK506-binding protein (FKBP), F_V, was fused to W199A TssL (Fig. 9A). FKBP are soluble signaling proteins that dimerize in response to a chemical inducer, rapamycin [44]. Hence, the couple F_V and AP20187, a non-toxic analogue of rapamycin, could be used for ligand-induced dimerization [44,45] (Fig. 9A). F_V was fused to the TssL C-terminus (Fig. 9A), which is located in the periplasm and permissive to insertion, as TssL subunits fused to peptidoglycan-binding motifs are commonly found associated with T6SS [32]. TOXCAT assay showed that the presence of AP20187 in the medium overcomes the dimerization defect caused by the

TssL^{TM} W199A mutation (Fig. 9B). Ligand-induced dimerization of the TssL W199A variant restores T6SS-mediated Hcp release (Fig. 9C) and antibacterial activity (Fig. 9D), and increases TssL W199A stability to wild-type levels (Fig. 9E-G). Taken together, these results demonstrate that Trp199 is a key residue for TssL^{TM} dimerization and that TssL^{TM} dimerization is essential for T6SS activity.

Discussion

In this study, we report that the TssL transmembrane segment is a major determinant of TssL dimerization. Using a combination of TOXCAT, NMR and MD assays, we show that TssL^{TM} dimer formation is mediated by π-π interactions involving three aromatic residues at the cytoplasmic side (Tyr184, Trp185 and Trp188) and one tryptophan at the periplasmic side (Trp199). We further provide evidence for a critical role of TM-mediated TssL dimerization in T6SS stability and activity.

Few data are available in the field of bacterial secretion systems regarding the role of TM segments, and more specifically how interactions between TM helices participate to the assembly of these multiprotein complexes. However, the dimerization of the *Agrobacterium tumefaciens* VirB10 protein TM helix is required for Type IV secretion [35,46].

Our results highlighted the specific and important role of TssL^{TM} aromatic residues in dimer formation. Interestingly, TssL^{TM} dimerization is mediated by a total of eight aromatic rings, with six of them forming a tight patch. π-π packing of aromatic rings is a common interaction motif in proteins [47,48], but is also a very common interface between proteins and ligands [49]. The involvement of aromatic-aromatic interactions in TM helices is not well documented [50]. By contrast, cation-π interactions, such as Lys-Trp interactions, have been shown to control TM interactions within the chloride intracellular channel protein 1 (CLIC1) [51]. Rather, tryptophan side-chains in TMH have usually functional roles including

selectivity or gatekeepers such as in conjugation coupling proteins [52] and proton or potassium channels [53-56], and locks for rotameric switches, such as for the ghrelin receptor [57]. Interestingly, an alignment of the TMH sequences of T6SS-associated TssL homologues covering the different T6SS subfamilies shows that tryptophan or aromatic residues are highly conserved at the N- and C-termini of the TMHs (Fig. 10). This conservation is also shared with T4bSS-associated IcmH/DotU proteins (Fig. 10), highlighting the importance of aromatic rings at these positions. It is noteworthy that, by contrast to the EAEC TssL TMH, only one aromatic residue is usually conserved at the N-terminus. This observation suggests that the packing between two aromatic rings might be sufficient to stabilize TssL TMH formation at the N-terminus, and thus may explain why single substitution of the Y184, W185 or W188 residue does not significantly impact dimer formation in the TOXCAT assay.

It is worthy to note that NMR H-D experiments did not fully copy the results of the TOXCAT assay. However, the MD simulations provided molecular explanations for all the discrepancies. First, no role of residue Thr194 in $TssL^{TM}$ dimerization could be inferred by H-D experiments, whereas the T194W substitution strongly interferes with dimerization using TOXCAT. However, MD simulations using a peptide corresponding to the T194W variant showed that this substitution induces a destabilization of the $TssL^{TM}$ dimer packing and a significant motion of one monomer relative to the other. Interestingly, the threonine side-chain tends to bend α-helices by the formation of an additional hydrogen bond between its side-chain γO atom and the i-3 or i-4 peptide carboxyl oxygen [58]. This additional hydrogen bond also alters the dynamic of the helix bending [59] in a way that, in the $TssL^{TM}$ peptide, opposes to the formation of a coiled-coil on the dimerization face. Hence, incorporating a small disturbance in bending flexibility at one side of the TMH results in a significant displacement of the residues located at the other side [58], such as we observed in the case of the $TssL^{TM}$ dimer. In conclusion, although Thr194 does not participate directly to the $TssL^{TM}$

interface, the additional hydrogen bond contributed by the side-chain is important to maintain the $TssL^{TM}$ in a conformation competent for dimerization. The quantitative TOX-CAT assays also indicated that several substitutions along the helix affect $TssL^{TM}$ dimer formation, albeit to a lower extent compared to T194W. While we did not conduct MD simulations for each variant, it is likely that these substitutions slightly impact $TssL^{TM}$ stability and/or conformation, and thus indirectly affect its dimerization. Second, the packing of the six aromatic rings (Tyr184, Trp185 and Trp188) at the N-terminal portion of the TssL α-helix is an important determinant of $TssL^{TM}$ dimerization, but none of the Y184W, W185A and W188A substitutions affects dimerization by TOXCAT. As noted above, the lack of effect of these single substitutions on TOXCAT can be explained by the redundancy of the π-π interactions between these aromatic rings, an hypothesis in agreement with the observation that only one aromatic residue is usually conserved at the $TssL^{TM}$ N-termini.

In between the N-terminal Tyr184, Trp185 and Trp188 and the C-terminal Trp199 residues of the dimer interface are located the three leucine residues ascertained as a potential leucine zipper. However, the TOXCAT assay showed that mutation of this potential leucine zipper did not impact $TssL^{TM}$ dimerization. Interestingly, contrarily to the prototypical motif found in the CGN4 leucine zipper [60], the structure of the $TssL^{TM}$ peptide revealed that it does not present a coiled-coil structure. As a consequence, the leucine side-chains point toward different directions and hence there is room to accommodate Trp substitutions owing to Trp flexibility due to the free rotation along the Cα-Cβ and Cβ-Cγ bonds.

The development of TssL-F_V fusions to control TssL dimer levels and hence T6SS assembly is a remarkable tool. Because the assembly of the TssJLM membrane complex represents an early stage of T6SS biogenesis [13,14,61], the ligand-inducible TssL dimerization could be used to synchronize T6SS assembly and activities.

Finally, a better understanding of the interactions between the TssL TMH provides the basis for the development of synthetic peptides that would inhibit TssL dimerization and thus T6SS assembly. Hydrophobic peptides interfering with transmembrane domains have been used to block the action of neuropilin-1, an actor of the human Hedgehog signalling pathway that is involved in development disorders and cancers [62,63]. TssL^{TM}-targeting peptides that mimick the dimerization interface might be of specific interest to diminish the virulence or the anti-bacterial activity of important bacterial pathogens that use the T6SS to colonize the host, such as *Vibrio cholerae*, *Pseudomonas aeruginosa*, or *Salmonella enterica* [64-68].

Material and Methods

Bacterial strains, media, growth conditions and chemicals

The bacterial strains used in this study are listed in Table S2. *Escherichia coli* K-12 DH5α, W3110 and NT326 [69] were used for cloning procedures, anti-bacterial competition and TOXCAT assays, respectively. The enteroaggregative *E. coli* strain 17-2 and its Δ*tssL* (previously described as Δ*sciP*; [20]) derivative were used for this study. Strains were routinely grown in LB at 37°C with aeration. The TOXCAT assay was performed in M9 minimal medium with glucose or maltose as carbon source. Expression of the T6SS gene cluster was induced in Sci1-inducing medium (SIM; M9 minimal medium supplemented with LB 10%, glycerol 0.4%, casaminoacids 40 µg.mL^{-1}, $MgCl_2$ 2 mM, $CaCl_2$ 0.1 mM, Vitamin B1 200 µg.mL^{-1} [70]). Plasmids and mutations were maintained by the addition of ampicillin (100 µg.mL^{-1} for *E. coli* K-12, 200 µg.mL^{-1} for EAEC) or kanamycin (50 µg.mL^{-1} for *E. coli* K-12). Protein synthesis was arrested by addition of spectinomycin (200 µg.mL^{-1}). Induction of genes cloned into pIBA vectors was obtained with anhydrotetracyclin (AHT – used at 0.02 µg.mL^{-1} throughout the study; IBA Technologies). The AP20187 dimerization inducer was purchased from Clinisciences and used at 20 mM. The anti-TolB polyclonal antibodies are from the laboratory collection while the anti-FLAG (clone M2, Sigma Aldrich) and anti-HA (clone HA-7, Sigma-Aldrich)

monoclonal antibodies and the goat secondary anti-mouse antibodies coupled to alkaline phosphatase (Jackson Immuno) or AlexaFluor® 680 (Molecular Probes) are commercially available.

Plasmid construction

The plasmids used in this study are listed in Table S2. Polymerase Chain Reactions (PCR) were performed with a Biometra thermocycler, using the Pfu Turbo DNA polymerase (Stratagene). Custom oligonucleotides were synthesized by Sigma-Aldrich and are listed in Table S2. Plasmids pIBA-TssL and pIBA-$TssL_C$ producing the full-length and the cytoplasmic domain (residues 1-183) of TssL protein fused to a N-terminal FLAG sequence have been previously described [25]. The sequence encoding the TssL transmembrane helix has been inserted into the pcckan vector [69] after PCR-amplification from the EAEC 17-2 chromosome DNA using primers 5-TssLTM-NheI and 3-TssLTM-BamHI. The *Nhe*I-*Bam*HI fragment was then inserted into pcckan digested by the same restriction enzymes to yield pcc-TssL-TM. FK506-binding protein (FKBP) fusion chimeras were engineered by a double PCR technique, allowing amplification of the FKBP(F36V) sequence (from plasmid pPSV35CV-ppkA-Fv; [45]) flanked by extensions annealing to the target vector [20,71]. The product of the first PCR has then been used as oligonucleotides for a second PCR using the pIBA-TssL or pcc-TssL-TM as template. Site-directed mutagenesis was performed using complementary oligonucleotides bearing the desired substitutions. All constructs have been verified by colony PCR, restriction analyses and DNA sequencing (Genome Express).

Antibacterial competition assay

The antibacterial growth competition assay was performed as previously described [43]. Briefly, the wild-type *E. coli* strain W3110 bearing the pUA66-*rrnB* plasmid (Kan^R [72]) was used as prey in the competition assay. The pUA66-*rrnB* plasmid provides a strong constitutive green fluorescent (GFP^+) phenotype. Attacker and prey cells were grown for 16 h in SIM medium, and then diluted in SIM to allow maximal expression of the *sci1* gene cluster [70]. Once the culture reached an absorbance at λ=600 nm (A_{600}) of 0.8, cells were harvested and normalized to A_{600}=10 in SIM. Attacker and prey cells were mixed to a 4:1 ratio and 20-µL drops of the mixture were spotted in triplicate onto a pre-

warmed dry SIM agar plate supplemented with 0.02 μg.mL^{-1} of AHT. After 4-hour incubation at 37°C, fluorescent images were recorded with a LI-COR Odyssey imager. The bacterial spots were scratched off, and cells were resuspended in LB medium and normalized to an A_{600}=0.5. Triplicates of 200 μL were transferred into wells of a black 96-well plate (Greiner) and the A_{600} and fluorescence (excitation, 485 nm; emission, 530 nm) were measured with a Tecan Infinite M200 microplate reader. The relative fluorescence was expressed as the intensity of fluorescence divided by the A_{600}, after subtracting the values of a blank sample. For estimating bacterial prey survival, colony-forming units (cfu) were enumerated after plating serial dilutions on LB plates supplemented with kanamycin. The experiments were done in triplicate, with identical results, and we report here the results of a representative experiment.

Hcp release assay

Supernatant and cell fractions have been separated as previously described [20] except that cells were grown in SIM medium. When necessary, AHT was added 30 minutes before harvesting the cells. Briefly, 2×10^9 cells producing HA epitope-tagged Hcp (from plasmid pOK-Hcp$_{HA}$; [20]) were harvested and collected by centrifugation at 2,000 × *g* for 5 min. The supernatant fraction was then subjected to a second low-speed centrifugation, a high-speed centrifugation (16,000 × *g* for 15 min) and filtered on sterile polyester membranes with a pore size of 0.2 μm (membrex 25 PET, membraPure GmbH) before precipitation with trichloroacetic acid (TCA) 15%. Cells and precipitated supernatant were resuspended in loading buffer and analysed by SDS-PAGE and immunoblotting with the anti-HA antibody. As control for cell lysis, Western blots were probed with antibodies raised against the periplasmic TolB protein.

TOXCAT assay

The TOXCAT assay was performed as described [33,34,69]. *MalE complementation assay*: NT326 cells producing the TOXCAT fusion were streaked onto M9 minimal medium plates supplemented with 0.4% glucose or with 0.4% maltose as the sole carbon source. Plates were incubated for 2 days at 37°C. *Disk diffusion assay*: 20 μL of chloramphenicol (90 mg.mL^{-1}) was added on a nitrocellulose 10-

mm filter disk (Bio-Rad, 0.2 µm pore size) disposed onto a sterile empty petri dish. After drying, the filter was deposited at the center of a dried LB plate supplemented with ampicillin. Plates were incubated for 6 hours at 37°C before removing the filter disk. 2 mL of a culture of NT326 cells producing the TOXCAT fusion were used to make a lawn and plates were incubated ON at 37°C. The experiments have been performed in triplicate. *TOXCAT quantitative assay*: NT326 cells producing the TOXCAT fusion were inoculated into 10 mL of LB supplemented with ampicillin and grown to an A_{600}=1 at 37°C with vigorous shaking. 10^{10} cells (~ 6 A_{600} units) were harvested by centrifugation and washed with 1 mL of sonication buffer (25 mM Tris-HCl, 2 mM EDTA, pH8.0). Cells were then resuspended in 1 mL of sonication buffer and lysed by sonication. *CAT activity measurements*: 12 µL of lysate were mixed with 300 µL of reaction buffer (0.1 mM acetyl-CoA, 0.4 mg.mL^{-1} 5,5'-dithiobis-(2-nitrobenzoic acid), 0.1 M Tris-HCl, pH7.8), and the absorbance was acquired at λ=412 nm at 10-sec intervals for a minimum of 4 min to measure the background rate of acetyl-CoA hydrolysis. Then, 12 µL of 2.5 mM chloramphenicol was added, and the absorbance was measured every 10 sec. for 1 min. Each lysate was assayed in triplicate, and the slopes of the recorded graphs were converted to enzyme activity units (ε= 13,600 at λ=412 nm).

AP20187-mediated FK506-binding protein dimerization

Dimerization of FKBP(F36V) was induced by the addition of 20 mM AP20187 (Clinisciences, resuspended in dimethylsulfoxide) in the culture medium.

Protein stability assay

Cultures were grown at 37°C to an A_{600} = 0.8, and 200 µg.mL^{-1} of spectinomycin was added to stop protein synthesis [73]. A sample was harvested at time zero and equivalent samples were harvested 5, 10, 15, 30, 60, 120, 240 and 480 min. after spectinomycin addition. The bacterial density was measured at different time points to verify that no growth occurred. Cell pellets were resuspended in Laemmli loading buffer, heated for 15 min at 96°C, and subjected to 12.5% SDS-PAGE. Western-blotting was performed with goat secondary anti-mouse antibodies coupled to AlexaFluor® 680 and

images were recorded at λ=700 nm using an LI-COR Odyssey imager. Image analyses were performed with the ImageJ processing program using the Fiji interface [74]. The image was first converted to grayscale in .jpg format. The rectangle tool of ImageJ was used to select a rectangular area of the size corresponding to the lane width, in order to cover the minimal area to contain the whole of the largest band. The same frame was used to select each TssL band of the nitrocellulose membrane. For each selection, the number of pixels was calculated. A control region with no band was also selected to subtract the background. The number of pixels of each band, relative to time 0 was then plotted against time. The degradation rate constant (k) was calculated as the slope of the linear curve obtained by plotting the Napierian logarithm of each intensity value against time and fitting to a first-order decay function. Half-life values ($\tau_{½}$) were obtained using the equation $\tau_{½}= \ln(2)/k$.

TssL^{TM} peptide synthesis and structural analysis by NMR

A synthetic peptide, corresponding to the TssL transmembrane segment (residues Met183-Ala207) with two additional lysine residues at the N- and C-terminus of the peptide (sequence: KKMYWLSWGAGIVTLAGLWCVLSSVLAKK) was synthesized by Schafer-N (Danemark). Two samples were prepared, one in H_2O and one in D_2O for proton/deuterium exchange experiments. For each sample 2 mg of peptide were solubilized in 500 µL of D25-Sodium Dodecyl Sulfate 1%, in 10 mM KH_2PO4, 1 mM D10-Dithiothreitol, pH 4.5. TOCSY and NOESY experiments were recorded at 300 K using a Bruker Avance III 600 spectrometer equipped with a TCI cryoprobe. Mixing time for the NOESY experiments was 300 ms. The NMR spectra were processed with Topsin software (Bruker) and proton assignment was obtained using the CARA software [75].

Molecular dynamics simulations

On the basis of NMR data, the sequence corresponding to the synthetic TssL peptide was modelled as a canonical α-helix using the Deepview software [76]. The structure was duplicated using VMD and a Tcl script was used to build 8 symmetric dimer conformations by translating and rotating monomers.

The resulting structures were in close contact and in parallel arrangements. A peptide-detergent complex was built using the Charmm-gui server [77]. The resulting micelles contained 112 SDS molecules and 17,600 water molecules. The system was neutralized using 112 Na^+ and 8 Cl^- ions. All the simulations were performed using Gromacs 5.1 with the Charmm 36 forcefield. For the simulations, the default protocol and MD parameters generated by Charmm-gui were conserved. Long range electrostatic forces were computed above 1.2 nm, and a switching function was used for short-range electrostatics forces between 1 and 1.2 nm. The system was minimized using the steepest descent algorithm until the maximum force converges under 1000 kJ/mol/nm. The micelle and the water environment around the peptide were relaxed using several rounds of simulations starting from constrained peptide, then relaxing forces on side-chains and finally on the main chain. The system was thermalized and equilibrated at 300 K using several rounds of simulation over 375 ps. A timestep of 1 fs, with the LINCS algorithm applied to constraint bonds that involves H atoms. The temperature was controlled using a multi-coupling scheme separating the peptide and the micelle, with an isotropic Berendsen thermostat and a coupling time constant of 5 ps and 1 ps for heating and equilibration respectively. For the production, a coupling scheme with 10-ns trajectories was produced for the various systems. The simulations were filtered on the basis of MD analysis, TOXCAT and NMR data that resulted on the selection of two simulations that were extended to 100 ns. Finally, simulations of the T194W variant were started from an equilibrated conformation of the wild-type peptide. MD simulations of Thr194 variants were performed after substitution of Thr194 by Trp on the TssL^{TM} structure using the Depview software for 20 ns respectively.

Acknowledgements

We thank Olivier Bornet and the NMR facilities of the Institut de Microbiologie de la Mediterranée for technical assistance in recording NMR experiments, Joseph Mougous (University of Washington, Seattle, USA) for providing the FKBP (F36V)-encoding plasmid

pPSV35CV-ppkA-Fv, Pierre Hubert, James Sturgis and members of the Cascales, Lloubès, Bouveret, Sturgis and Cambillau research groups for discussions, Molly Ba, Isabelle Bringer, Annick Brun, and Oliver Uderso for technical assistance, Matt Edessin for encouragements, and the four anonymous referees for their constructive comments and suggestions. This work was supported by the Aix-Marseille Université (AMU), the Centre National de la Recherche Scientifique (CNRS), and grants from the Agence Nationale de la Recherche (ANR-14-CE14-0006-02) and the European Society for Clinical Microbiology and Infectious Diseases (ESCMID) to E.C. and E.D., respectively. The MD simulations were performed using the high performance computing (HPC) resources from the Grand Equipement National de Calcul Intensif of the Centre Informatique National de l'Enseignement Supérieur (GENCI-CINES grant 2016077044). A.Z. was supported by a doctoral fellowship from the French Ministère de la Recherche and a Fondation pour la Recherche Médicale end-of-thesis fellowship (FDT20140931060). E.D. is supported by the Institut National de la Santé et de la Recherche Médicale (INSERM).

References

[1] F. Boyer, G. Fichant, J. Berthod, Y. Vandenbrouck, I. Attree, Dissecting the bacterial type VI secretion system by a genome wide in silico analysis: what can be learned from available microbial genomic resources?, BMC Genomics 10 (2009) 104.

[2] J.M. Silverman, Y.R. Brunet, E. Cascales, J.D. Mougous, Structure and regulation of the type VI secretion system, Ann. Rev. Microbiol. 66 (2012) 453–472.

[3] A.B. Russell, S.B. Peterson, J.D. Mougous, Type VI secretion system effectors: poisons with a purpose, Nat. Rev. Microbiol. 12 (2014) 137–148.

[4] E. Durand, C. Cambillau, E. Cascales, L. Journet, VgrG, Tae, Tle, and beyond: the versatile arsenal of type VI secretion effectors, Trends Microbiol. 22 (2014) 498–507.

[5] F.R. Cianfanelli, L. Monlezun, S.J. Coulthurst, Aim, load, fire: the type VI secretion system, a bacterial nanoweapon, Trends Microbiol. 24 (2016) 51–62.

[6] A. Hachani, T.E. Wood, A. Filloux, Type VI secretion and antihost effectors, Curr. Opin. Microbiol. 29 (2015) 81–93.

[7] A. Zoued, Y.R. Brunet, E. Durand, M.S. Aschtgen, L. Logger, B. Douzi, L. Journet, C. Cambillau, E. Cascales, Architecture and assembly of the type VI secretion system, Biochim. Biophys. Acta 1843 (2014) 1664–1673.

[8] B.T. Ho, T.G. Dong, J.J. Mekalanos, A view to a kill: the bacterial Type VI secretion system, Cell Host Microbe 15 (2014) 9–21.

[9] M. Basler, Type VI secretion system: secretion by a contractile nanomachine, Philos. Trans. R. Soc. Lond. Ser. B Biol. Sci. 370 (2015) 1679.

[10] M. Basler, M. Pilhofer, G.P. Henderson, G.J. Jensen, J.J. Mekalanos, Type VI secretion requires a dynamic contractile phage tail-like structure, Nature 483 (2012) 182–186.

[11] M. Basler, B.T. Ho, J.J. Mekalanos, Tit-for-tat: type VI secretion system counterattack during bacterial cell–cell interactions, Cell 152 (2013) 884–894.

[12] Y.R. Brunet, L. Espinosa, S. Harchouni, T. Mignot, E. Cascales, Imaging type VI secretion-mediated bacterial killing, Cell Rep. 3 (2013) 36–41.

[13] Y.R. Brunet, A. Zoued, F. Boyer, B. Douzi, E. Cascales, The type VI secretion TssEFGK-VgrG phage-like baseplate is recruited to the TssJLM membrane complex via multiple contacts and serves as assembly platform for tail tube/sheath polymerization, PLoS Genet. 15 (3) (2015) e1005545.

[14] E. Durand, V.S. Nguyen, A. Zoued, L. Logger, G. Péhau-Arnaudet, M.S. Aschtgen, S. Spinelli, A. Desmyter, B. Bardiaux, A. Dujeancourt, A. Roussel, C. Cambillau, E. Cascales, R. Fronzes, Biogenesis and structure of a type VI secretion membrane core complex, Nature 523 (2015) 555–560.

[15] A. Zoued, E. Durand, C. Bebeacua, Y.R. Brunet, B. Douzi, C. Cambillau, E. Cascales, L. Journet, TssK is a trimeric cytoplasmic protein interacting with components of both phage-like and membrane anchoring complexes of the Type VI secretion system, J. Biol. Chem. 288 (2013) 27031–27041.

[16] L. Logger, M.S. Aschtgen, M. Guérin, E. Cascales, E. Durand, Molecular dissection of the interface between the Type VI secretion TssM cytoplasmic domain and the TssG baseplate component, J Mol Biol. 428 (2016) 4424–4437.

[17] A. Zoued, C.J. Cassaro, E. Durand, B. Douzi, A.P. España, C. Cambillau, L. Journet, E. Cascales, Structure-function analysis of the TssL cytoplasmic domain reveals a new interaction between the Type VI secretion baseplate and membrane complexes, J Mol Biol. 428 (2016) 4413–4423.

[18] V.S. Nguyen, L. Logger, S. Spinelli, P. Legrand, T.T. Huyen Pham, T.T. Nhung Trinh, Y. Cherrak, A. Zoued, A. Desmyter, E. Durand, A. Roussel, C. Kellenberger, E. Cascales, C. Cambillau, Type VI secretion TssK baseplate protein exhibits structural similarity with phage receptor-binding proteins and evolved to bind the membrane complex, Nat Microbiol 2 (2017) 17103.

[19] M.S. Aschtgen, C.S. Bernard, S. De Bentzmann, R. Lloubès, E. Cascales, SciN is an outer membrane lipoprotein required for type VI secretion in enteroaggregative *Escherichia coli*, J. Bacteriol. 190 (2008) 7523–7531.

[20] M.S. Aschtgen, M. Gavioli, A. Dessen, R. Lloubès, E. Cascales, The SciZ protein anchors the enteroaggregative *Escherichia coli* type VI secretion system to the cell wall, Mol. Microbiol. 75 (2010) 886–899.

[21] C. Felisberto-Rodrigues, E. Durand, M.S. Aschtgen, S. Blangy, M. Ortiz-Lombardia, B. Douzi, C. Cambillau, E. Cascales, Towards a structural comprehension of bacterial type VI secretion systems: characterization of the TssJ–TssM complex of an *Escherichia coli* pathovar, PLoS Pathogens. 7 (2011) e1002386.

[22] V.A. Rao, S.M. Shepherd, G. English, S.J. Coulthurst, W.N. Hunter, The structure of *Serratia marcescens* Lip, a membrane-bound component of the type VI secretion system, Acta Crystallogr D Biol Crystallogr. 67 (2011) 1065–1072.

[23] C.S. Robb, M. Assmus, F.E. Nano, A.B. Boraston, Structure of the T6SS lipoprotein TssJ1 from *Pseudomonas aeruginosa*. Acta Crystallogr Sect F Struct Biol Cryst Commun. 69 (2013) 607–610.

[24] L.S. Ma, J.S. Lin, E.M. Lai, An IcmF family protein, ImpLM, is an integral inner membrane protein interacting with ImpKL, and its walker a motif is required for type VI secretion systemmediated hcp secretion in Agrobacterium tumefaciens, J. Bacteriol. 191 (2009) 4316–4129.

[25] M.S. Aschtgen, A. Zoued, R. Lloubès, L. Journet, E. Cascales, The C-tail anchored TssL subunit, an essential protein of the enteroaggregative Escherichia coli Sci-1 type VI secretion system, is inserted by YidC, Microbiologyopen 1 (2012) 71–82.

[26] E. Pross, L. Soussoula, I. Seitl, D. Lupo, A. Kuhn, Membrane targeting and insertion of the C-tail protein SciP, J Mol Biol. 428 (2016) 4218–4227.

[27] E. Durand, A. Zoued, S. Spinelli, P.J. Watson, M.S. Aschtgen, L. Journet, C. Cambillau, E. Cascales, Structural characterization and oligomerization of the TssL protein, a component shared by bacterial type VI and type IVb secretion systems, J. Biol. Chem. 287 (2012) 14,157–14,168.

[28] C.S. Robb, F.E. Nano, A.B. Boraston, The structure of the conserved type six secretion protein TssL (DotU) from *Francisella novicida*, J Mol Biol. 419 (2012) 277–283.

[29] J.H. Chang, Y.G. Kim, Crystal structure of the bacterial type VI secretion system component TssL from *Vibrio cholerae*, J Microbiol. 53 (2015) 32–37.

[30] B.S. Weber, S.W. Hennon, M.S. Wright, N.E. Scott, V. de Berardinis, L.J. Foster, J.A. Ayala, M.D. Adams, M.F. Feldman, Genetic dissection of the Type VI secretion system in *Acinetobacter* and identification of a novel peptidoglycan hydrolase, TagX, required for its biogenesis, MBio. 7 (2016) e01253-16.

[31] Y.G. Santin, E. Cascales, Domestication of a housekeeping transglycosylase for assembly of a Type VI secretion system, EMBO Rep. 18 (2017) 138–149.

[32] M.S. Aschtgen, M.S. Thomas, E. Cascales, Anchoring the type VI secretion system to the peptidoglycan: TssL, TagL, TagP... what else?, Virulence. 1 (2010) 535–540.

[33] W.P. Russ, D.M. Engelman, TOXCAT: a measure of transmembrane helix association in a biological membrane, Proc Natl Acad Sci U S A. 96 (1999) 863–868.

[34] L. Logger, A. Zoued, E. Cascales, Fusion reporter approaches to monitoring transmembrane helix interactions in bacterial membranes, Methods Mol Biol. 1615 (2017) 199–210.

[35] J. Garza, P.J. Christie, A putative transmembrane leucine zipper of *Agrobacterium* VirB10 is essential for T-pilus biogenesis but not type IV secretion, J Bacteriol. 195 (2013) 3022–3034.

[36] L.L. Sharp, J. Zhou, D.F. Blair, Features of MotA proton channel structure revealed by tryptophan-scanning mutagenesis, Proc Natl Acad Sci U S A. 92 (1995) 7946–7950.

[37] D.V. Tulumello, C.M. Deber, SDS micelles as a membrane-mimetic environment for transmembrane segments, Biochemistry. 48 (2009) 12096–12103.

[38] J. Venkatraman, G.A. Nagana Gowda, P. Balaram, Structural analysis of synthetic peptide fragments from EmrE, a multidrug resistance protein, in a membrane-mimetic environment, Biochemistry. 41 (2002) 6631–6639.

[39] Y. Wu, S.C. Shih, N.K. Goto, Probing the structure of the Ff bacteriophage major coat protein transmembrane helix dimer by solution NMR, Biochim Biophys Acta. 1768 (2007) 3206–3215.

[40] J.H. Chill, J.M. Louis, C. Miller, A. Bax, NMR study of the tetrameric KcsA potassium channel in detergent micelles, Protein Sci. 15 (2006) 684–698.

[41] K. Wuthrich, NMR of proteins and nucleic acids, Ed. Wiley (1986)

[42] E. Cascales, The type VI secretion toolkit, EMBO Rep. 9 (2008) 735–741.

[43] N. Flaugnatti, T.T. Le, S. Canaan, M.S. Aschtgen, V.S. Nguyen, S. Blangy, C. Kellenberger, A. Roussel, C. Cambillau, E. Cascales, L. Journet, A phospholipase A1 anti-bacterial T6SS effector interacts directly with the C-terminal domain of the VgrG spike protein for delivery. Mol Microbiol. 99 (2016) 1099–1118.

[44] T.W. Corson, N. Aberle, C.M. Crews, Design and applications of bifunctional small molecules: why two heads are better than one, ACS Chem Biol. 3 (2008) 677–692.

[45] F. Hsu, S. Schwarz, J.D. Mougous, TagR promotes PpkA-catalysed type VI secretion activation in *Pseudomonas aeruginosa*, Mol Microbiol. 72 (2009) 1111–1125.

[46] S.J. Jakubowski, J.E. Kerr, I. Garza, V. Krishnamoorthy, R. Bayliss, G. Waksman, P.J. Christie, *Agrobacterium* VirB10 domain requirements for type IV secretion and T pilus biogenesis, Mol Microbiol. 71 (2009) 779–794.

[47] R. Anjana, M.K. Vaishnavi, D. Sherlin, S.P. Kumar, K. Naveen, P.S. Kanth, K. Sekar, Aromatic-aromatic interactions in structures of proteins and protein-DNA complexes: a study based on orientation and distance, Bioinformation. 8 (2012) 1220–1224.

[48] D.E. Robillard, P.T. Mpangase, S. Hazelhurst, F. Dehne, SpeeDB: fast structural protein searches, Bioinformatics. 31 (2015) 3027–3034.

[49] S. Li, Y. Xu, Q. Shen, X. Liu, J. Lu, Y. Chen, T. Lu, C. Luo, X. Luo, M. Zheng, H. Jiang, Non-covalent interactions with aromatic rings: current understanding and implications for rational drug design, Curr Pharm Des. 19 (2013) 6522–6533.

[50] R.M. Johnson, K. Hecht, C.M. Deber, Aromatic and cation-pi interactions enhance helix-helix association in a membrane environment, Biochemistry. 46 (2007) 9208–9214.

[51] B. Peter, A.A. Polyansky, S. Fanucchi, H.W. Dirr, A Lys-Trp cation-π interaction mediates the dimerization and function of the chloride intracellular channel protein 1 transmembrane domain, Biochemistry. 53 (2014) 57–67.

[52] I. Tato, S. Zunzunegui, F. de la Cruz, E. Cabezon, TrwB, the coupling protein involved in DNA transport during bacterial conjugation, is a DNA-dependent ATPase, Proc Natl Acad Sci U S A. 102 (2005) 8156–8161.

[53] J.K. Williams, Y. Zhang, K. Schmidt-Rohr, M. Hong, pH-dependent conformation, dynamics, and aromatic interaction of the gating tryptophan residue of the influenza M2 proton channel from solid-state NMR, Biophys J. 104 (2013) 1698–1708.

[54] R. Männikkö, P.J. Stansfeld, A.S. Ashcroft, A.T. Hattersley, M.S. Sansom, S. Ellard, F.M. Ashcroft, A conserved tryptophan at the membrane-water interface acts as a gatekeeper for Kir6.2/SUR1 channels and causes neonatal diabetes when mutated, J Physiol. 589 (2011) 3071–3083.

[55] Y. Wu, G.A. Voth, Computational studies of proton transport through the M2 channel, FEBS Lett. 552 (2003) 23–27.

[56] L. Garneau, H. Klein, M.F. Lavoie, E. Brochiero, L. Parent, R. Sauvé, Aromatic-aromatic interactions between residues in KCa3.1 pore helix and S5 transmembrane segment control the channel gating process, J Gen Physiol. 143 (2014) 289–307.

[57] B. Holst, R. Nygaard, L. Valentin-Hansen, A. Bach, M.S. Engelstoft, P.S. Petersen, T.M. Frimurer, T.W. Schwartz, A conserved aromatic lock for the tryptophan rotameric switch in TM-VI of seven-transmembrane receptors, J Biol Chem. 285 (2010) 3973–3985.

[58] J.A. Ballesteros, X. Deupi, M. Olivella, E.E. Haaksma, L. Pardo, Serine and threonine residues bend alpha-helices in the chi(1) = g(-) conformation, Biophys J. 79 (2000) 2754–2760.

[59] C. Del Val, S.H. White, A.N. Bondar, Ser/Thr motifs in transmembrane proteins: Conservation patterns and effects on local protein structure and dynamics. J Membr. Biol. 245 (2012) 717–730.

[60] E.K. O'Shea, J.D. Klemm, P.S. Kim, T. Alber, X-ray structure of the GCN4 leucine zipper, a two-stranded, parallel coiled coil, Science 254 (1991) 539–44.

[61] A.J. Gerc, A. Diepold, K. Trunk, M. Porter, C. Rickman, J.P. Armitage, N.R. Stanley-Wall, S.J. Coulthurst, Visualization of the *Serratia* Type VI secretion system reveals unprovoked attacks and dynamic assembly, Cell Rep. 12 (2015) 2131–2142.

[62] L. Roth, C. Nasarre, S. Dirrig-Grosch, D. Aunis, G. Crémel, P. Hubert, D. Bagnard, Transmembrane domain interactions control biological functions of neuropilin-1, Mol Biol Cell. 19 (2008) 646–654.

[63] P. Hubert, P. Sawma, J.P. Duneau, J. Khao, J. Hénin, D. Bagnard, J. Sturgis, Single-spanning transmembrane domains in cell growth and cell-cell interactions: More than meets the eye?, Cell Adh Migr. 4 (2010) 313–324.

[64] A. Joshi, B. Kostiuk, A. Rogers, J. Teschler, S. Pukatzki, F.H. Yildiz, Rules of engagement: the Type VI secretion system in *Vibrio cholerae*, Trends Microbiol. 25 (2017) 267–279.

[65] T.G. Sana, B. Berni, S. Bleves, The T6SSs of *Pseudomonas aeruginosa* strain PAO1 and their effectors: beyond bacterial-cell targeting, Front Cell Infect Microbiol. 6 (2016) 61.

[66] J. Klockgether, B. Tümmler, Recent advances in understanding *Pseudomonas aeruginosa* as a pathogen, F1000Res. 6 (2017) 1261.

[67] T.G. Sana, N. Flaugnatti, K.A. Lugo, L.H. Lam, A. Jacobson, V. Baylot, E. Durand, L. Journet, E. Cascales, D.M. Monack, *Salmonella* Typhimurium utilizes a T6SS-mediated antibacterial weapon to establish in the host gut, Proc Natl Acad Sci U S A. 113 (2016) E5044–5051.

[68] W. Zhao, F. Caro, W. Robins, J.J. Mekalanos, Antagonism toward the intestinal microbiota and its effect on *Vibrio cholerae* virulence, Science. 359 (2018) 210–213.

[69] W.P. Russ, D.M. Engelman, The GxxxG motif: a framework for transmembrane helix-helix association, J Mol Biol. 296 (2000) 911–919.

[70] Y.R. Brunet, C.S. Bernard, M. Gavioli, R. Lloubes, E. Cascales, An epigenetic switch involving overlapping Fur and DNA methylation optimizes expression of a type VI secretion gene cluster, PLoS Genetics 7 (2011) e1002205.

[71] F. van den Ent, J. Lowe, RF cloning: a restriction-free method for inserting target genes into plasmids, J. Biochem. Biophys. Meth. 67 (2006) 67–74.

[72] A. Zaslaver, A. Bren, M. Ronen, S. Itzkovitz, I. Kikoin, S. Shavit, W. Liebermeister, M.G. Surette, U. Alon, A comprehensive library of fluorescent transcriptional reporters for *Escherichia coli*, Nat Methods. 3 (2006) 623–628.

[73] E. Cascales, R. Lloubès, J.N. Sturgis, The TolQ-TolR proteins energize TolA and share homologies with the flagellar motor proteins MotA-MotB, Mol Microbiol. 42 (2001) 795–807.

[74] J. Schindelin, I. Arganda-Carreras, E. Frise, V. Kaynig, M. Longair, T. Pietzsch, S. Preibisch, C. Rueden, S. Saalfeld, B. Schmid, J.Y. Tinevez, D.J. White, V. Hartenstein, K. Eliceiri, P. Tomancak, A. Cardona A, Fiji: an open-source platform for biological-image analysis, Nat Methods. 9 (2012) 676–682.

[75] R. Keller, Computer aided resonance assignment tutorial, (2014) http://cara.nmr.ch/

[76] N. Guex, M.C. Peitsch, SWISS-MODEL and the Swiss-PdbViewer: an environment for comparative protein modeling, Electrophoresis 18 (1997) 2714–2723

[77] S. Jo, J.B. Lim, J.B. Klauda, W. Im, CHARMM-GUI membrane builder for mixed bilayers and its application to yeast membranes, Biophys J. 97 (2009) 50–58.

Legend to Figures

Figure 1. Schematic representation of the T6SS membrane complex and TssJLM proteins. (A) Representation of the T6SS highlighting the cytoplasmic tail structure anchored to the cell envelope by the membrane complex. (B) Negative-stain electron microscopy structural model of the TssJLM membrane complex [14]. (C) Localisation, topology and structure of the TssJ outer membrane lipoprotein, and of the TssL and TssM inner membrane proteins. IM, inner membrane; OM, outer membrane.

Figure 2. TssL^{TM} dimerizes. TOXCAT assay. NT316 reporter cells producing the indicated ToxR-X-MBP fusions (empty, no TMH sequence cloned; GpA^{TM}, Glycophorin A TMH; GpA$^{TM(G83I)}$, GpA^{TM} with G83I substitution; TssL^{TM}, TssL TMH) were streaked on M9 minimal medium supplemented with glucose (A) or maltose (B) as sole carbon source.

Resistance to chloramphenicol (cam) conferred by the TM-mediated dimerization of the ToxR transcriptional regulator was measured by the disk assay (C, halo diameter mean ± standard deviation [SD] in mm) and quantitative chloramphenicol acetyltransferase (Cat) assay (D). The mean (value relative to the value obtained for the "empty" vector) is indicated on top on each bar.

Figure 3. Thr194 and Trp199 contribute to TssL^{TM} dimerization. (A) Sequence of the TssL^{TM} peptide. The numbering is relative to the full-length TssL protein. The transmembrane segment is indicated by the green frame and the leucine residues participating to a putative leucine zipper are coloured red. The two leucine residues substituted in the LALA mutant ware underlined. (B) TOXCAT disk assay of the TssL^{TM} fragment and its LALA derivative. The diameter of the halo is indicated on bottom (mean ± SD in mm). The quantitative Cat assay measures are reported in panel D. TOXCAT disk (C) and quantitative Cat (D) assays of the TssL^{TM} fragments bearing the indicated substitutions. The level of activity corresponding to the empty plasmid is indicated by the red dotted line.

Figure 4. TM-mediated contacts stabilize TssL dimer on SDS-PAGE. 2× 10^8 Δ*tssL* cells producing FLAG-tagged full-length TssL or the indicated TssL variants (TssL$_C$, cytoplasmic domain of TssL; T194W and W199A, substitution variants of the TM Thr194 and Trp199 residues respectively) were subjected to 12.5% SDS-PAGE and immunoblotting with the monoclonal anti-FLAG antibody. The position of TssL, TssL$_C$ and TssL dimers (*) are indicated on right. Molecular weight markers are indicated on left.

Figure 5. The Trp185 and Trp199 rings are protected in NMR Hydrogen-Deuterium exchange experiments. (A) Zoom-in of the H_N/H_N region of the NOESY spectrum of the TssL^{TM} peptide (2 mM) at 300K. The NMR sample was in phosphate buffer pH4.5 and SDS

1% (H_2O conditions). Cross peaks (nuclear Overhauser effects) corresponding to coupling between H_N of residues i and i+1 are observed. The assignment is shown in Table S1 and Fig. S1. (B and C) Overlay of the NOESY spectra of the TssL^{TM} peptide in H_2O (blue) and D_2O (red). H_N chemical shift assignment was indicated by residues sequence numbering. In D_2O, the exposed protons are exchanged with Deuterium and thus disappeared; however the protected protons are not exchanged and thus are still observable. In (B) the regions of H_N (x axis)/ H_{CA} (y axis) correlations is shown, and in (C) H_N of rings of tryptophan residues are shown. (D) Sequence of the TssL^{TM} peptide. The numbering is relative to the full-length TssL protein. The transmembrane segment is indicated by the green frame, and the tryptophan residues protected in H-D exchange experiments (Trp185 and Trp199) are coloured red. (E) Structural model of the TssL^{TM} monomer in SDS micelles. The orientation of the transmembrane segment relative to the membrane is shown. Residues located at the TssL^{TM} interface (indicated on right), as well as residue Thr194 are represented by spheres (tryptophan residues in grey, leucine zipper residues in pink). (F) Representation of the structural model of TssL^{TM} dimer in SDS micelles obtained by MD simulations of the TssL^{TM} monomer. The orientation of the two transmembrane segments relative to the membrane is shown. The Trp185, Trp188 and Trp199 rings are represented by spheres and pointed with arrowheads, highlighting the packing of the two Trp199 rings at the periplasmic side and of the four rings from Trp185 and Trp188 at the cytoplasmic side.

Figure 6. The Trp185 and Trp199 rings control tight packing of the TssL^{TM} dimer. (A) Superimposition of the averaged structures of TssL^{TM} monomerA obtained from the molecular dynamic simulations of 8 different TssL^{TM} dimers. The Thr194 and Trp199 residues are shown in spheres. (B and C) For the eight simulations of the dimer, (labeled from 0° to 350°), the superimposed structure of monomer A (ribbon) is represented at the center. The Thr194 and Trp199 side chains corresponding to the reference simulation (0°) are shown

in spheres. The trajectory traces of the Thr194 (B) and Trp199 (C) side chains of monomer B are shown at the periphery of the central helix. (D and E) Top panels: distances (in nm) between the two residues Y184 (black), Trp185 (red), Trp188 (green), Thr194 (blue), or Trp199 (yellow) in the dimer during 100-ns MD simulations starting from the 0° (D) and 350° (E) conformations. Bottom panels: final structures obtained after the 100-ns MD simulations starting from the 0° (D) and 350° (E) conformations. Residues are shown in spheres with the same color code than top panels.

Figure 7. Trp199 is required for T6SS function. (A) Hcp release assay. The cell pellet (C) and supernatant (S) fractions from 5× 10^8 cells of the wild-type 17-2 or Δ*tssL* derivative, or Δ*tssL* producing FLAG-tagged full-length TssL (*tssL*+) or the indicated TssL variants, and HA-tagged Hcp, were subjected to 12.5% SDS-PAGE and immunoblotted with anti-TolB (periplasmic leakage control, upper panel), anti-HA (to detect Hcp, middle panel) and anti-FLAG (to detect TssL, lower panel) antibodies. Molecular weigh markers are indicated on the left. (B) Anti-bacterial activity. The indicated attacker strains were mixed with kanamycin resistant GFP^+ prey cells and spotted on SIM medium. After incubation, the fluorescent image of the spot was recorded (middle panel) and level of surviving prey cells was estimated by measuring the fluorescence (upper graph) and by counting the number of colonies on kanamycin plates (lower graph).

Figure 8. Trp199 stabilizes TssL. (A) 5× 10^8-cell samples of the Δ*tssL* strain producing FLAG-tagged full-length TssL or the indicated TssL variants were harvested at the indicated time (in min) after protein synthesis arrest and were subjected to 12.5% SDS-PAGE and immunoblotting with anti-FLAG antibody, and secondary antibody coupled to AlexaFluor 680. Molecular weigh markers are indicated on the left. The relative intensity of each band

was plotted against time (B) and half-times of TssL and TssL variants (in min) were calculated from the slope of the first-order decay function (C).

Figure 9. Trp199-mediated TssL^{TM} dimerization is required for TssL stability and T6SS function. (A) Schematic representation of the TssL-W199A-F_V chimera protein. The TssL full-length protein carrying the W199A substitution (schematized with the red star) was fused to the FKBP F36V variant domain (F_V, green). F_V dimerization could be induced by the rapamycin homologue AP20187 (AP, pink diamond). P, periplasm; C, cytoplasm. (B) TOXCAT disk (upper panel) and quantitative Cat (lower panel) assays of W199A TssL^{TM} fused to F_V (W199A-F_V) in absence (-) or presence (+) of the FKBP ligand inducer AP20187 (AP). (C) Hcp release assay. The cell pellet (C) and supernatant (S) fractions from 5× 10^8 Δ*tssL* cells producing FLAG-tagged W199A-F_V and HA-tagged Hcp, grown in absence (-) or presence (+) of AP were subjected to 12.5% SDS-PAGE and immunoblotted with anti-TolB (periplasmic leakage control, upper panel), anti-HA (to detect Hcp, middle panel) and anti-FLAG (to detect TssL-F_V, lower panel) antibodies. Molecular weigh markers are indicated on the left. (D) Anti-bacterial activity. The Δ*tssL* attacker strain producing W199A-F_V was mixed with kanamycin resistant GFP^+ prey cells and spotted on SIM medium supplemented (+) or not (-) with AP. After incubation, the fluorescent image of the spot was recorded (middle panel) and level of surviving prey cells was estimated by measuring the fluorescence (upper graph) and by counting the number of colonies on kanamycin plates (lower graph). (E) 5× 10^8-cell samples of the Δ*tssL* strain producing TssL-W199A-F_V, grown in absence (-) or presence (+) of AP were harvested at the indicated time (in min) after protein synthesis arrest and were subjected to 12.5% SDS-PAGE and immunoblotting with anti-FLAG antibody, and secondary antibody coupled to AlexaFluor® 680. Molecular weigh markers are indicated on the left. The relative intensity of each TssL-F_V band was plotted against time (F) and half-times of W199A-F_V were calculated from the slope of the first-order decay function (G).

Figure 10. Sequence alignment of the TMHs from selected TssL homologues. The sequences of the TMHs of the T6SS-associated TssL proteins and T4bSS-associated IcmH/DotU proteins from strains listed on left (phylogeny realised based on the full-length TssL/IcmH sequences using the server at www.phylogeny.fr) were aligned using Clustal W (right panel). The position of the TMH (from experimental data for EAEC [25] or identified using the TMHMM and TMPred TMH prediction servers) is underlined in green. Tryptophan and other aromatic residues located at the N- and C-termini of the TMH sequences are indicated in red and blue respectively. The residues participating in π-π packing for EAEC TssL TMH dimerization (Y184, W185, W188 and W199; this study) are underlined.

Legend to Supplementary Figures

Supplementary Figure S1. Assignment of the TssL^{TM} NOESY spectrum. The H_N/H_N region of the NOESY spectrum of the TssL^{TM} peptide in H_2O is shown (same as Fig. 5A). The cross peak correlations are indicated by sequential numbering of the TssL^{TM} residues.

Supplementary Figure S2. Instability in the TssL^{TM} T194W mutant. (A) Contact map for the TssL^{TM} dimer (left) and the T194W mutant dimer (right). (B and C) Lateral (B, left panel) and top (B, right panel) views and root mean square deviation (RMSD, in Å) (C) of the orientation of monomer B relative to the fixed monomer A during the course of the 20-ns molecular dynamics simulation of the T194W mutant.

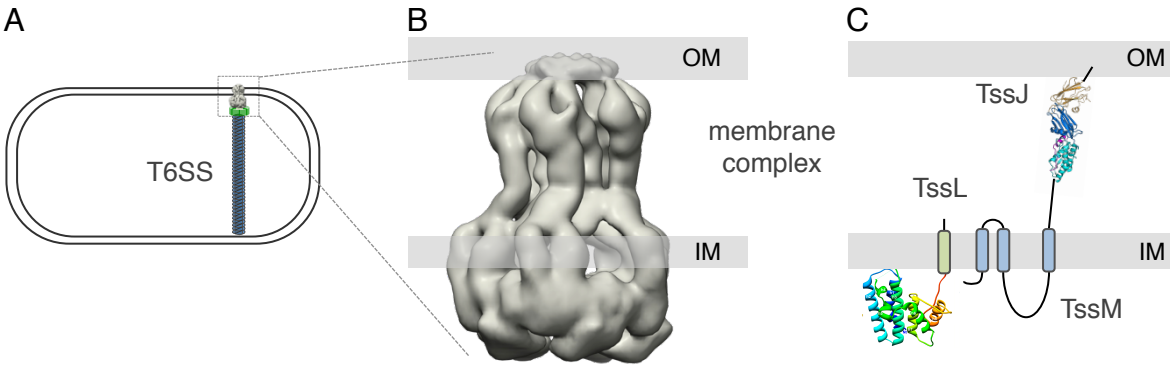

Figure 1

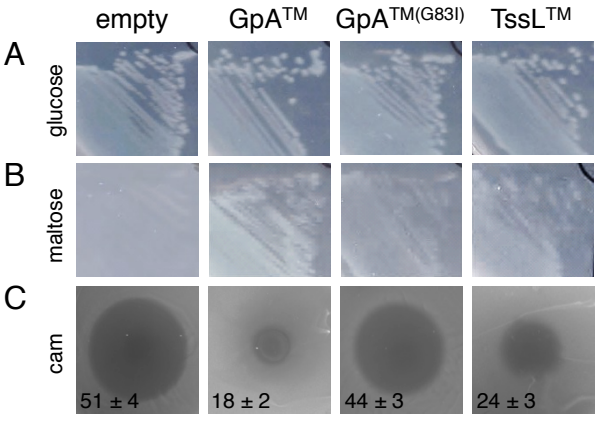
empty
GpA^TM
GpA^TM(G83I)
TssL^TM
A
glucose
B
maltose
C
cam
51 ± 4
18 ± 2
44 ± 3
24 ± 3

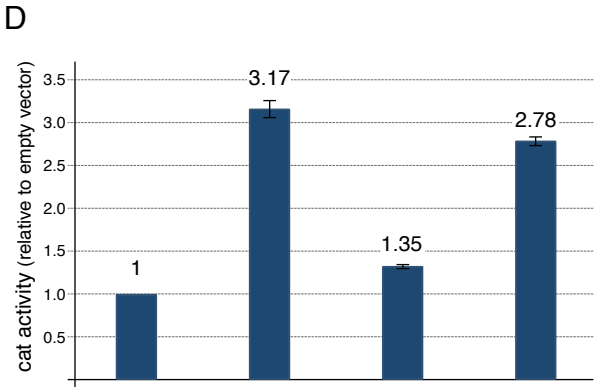
D
cat activity (relative to empty vector)
3.5
3.0
2.5
2.0
1.5
1.0
0.5
1
3.17
1.35
2.78

Figure 2

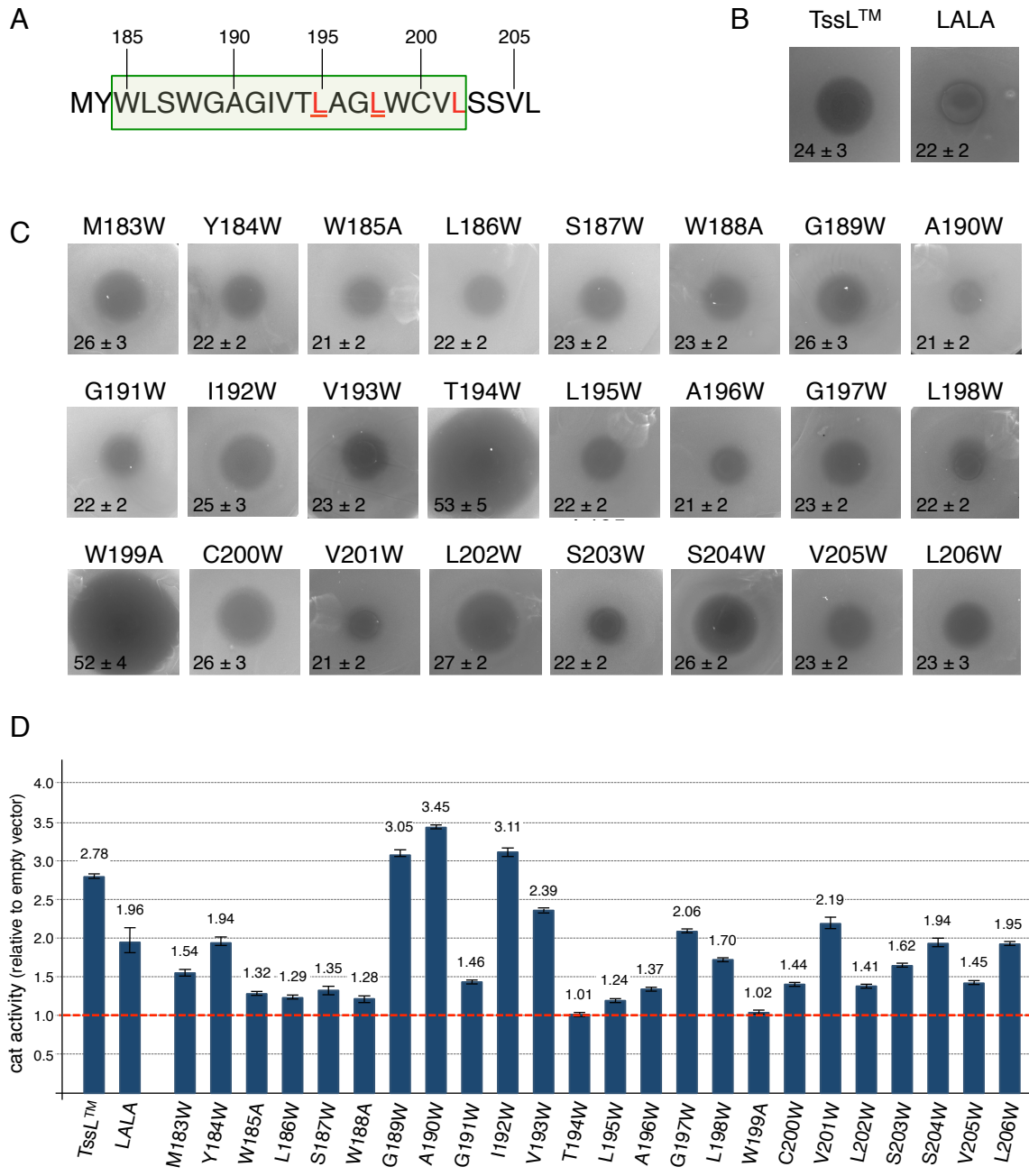
A
185
190
195
200
205
MYWLSWGAGIVTLAGLWCVLSSVL
B
TssL™
LALA
24 ± 3
22 ± 2
C
M183W
Y184W
W185A
L186W
S187W
W188A
G189W
A190W
26 ± 3
22 ± 2
21 ± 2
22 ± 2
23 ± 2
23 ± 2
26 ± 3
21 ± 2
G191W
I192W
V193W
T194W
L195W
A196W
G197W
L198W
22 ± 2
25 ± 3
23 ± 2
53 ± 5
22 ± 2
21 ± 2
23 ± 2
22 ± 2
W199A
C200W
V201W
L202W
S203W
S204W
V205W
L206W
52 ± 4
26 ± 3
21 ± 2
27 ± 2
22 ± 2
26 ± 2
23 ± 2
23 ± 3
D
cat activity (relative to empty vector)
4.0
3.5
3.0
2.5
2.0
1.5
1.0
0.5
2.78
1.96
1.54
1.94
1.32
1.29
1.35
1.28
3.05
3.45
1.46
3.11
2.39
1.01
1.24
1.37
2.06
1.70
1.02
1.44
2.19
1.41
1.62
1.94
1.45
1.95
TssL™
LALA
M183W
Y184W
W185A
L186W
S187W
W188A
G189W
A190W
G191W
I192W
V193W
T194W
L195W
A196W
G197W
L198W
W199A
C200W
V201W
L202W
S203W
S204W
V205W
L206W

Figure 3

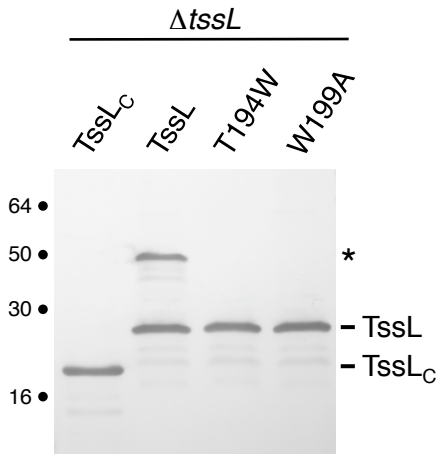

Figure 4

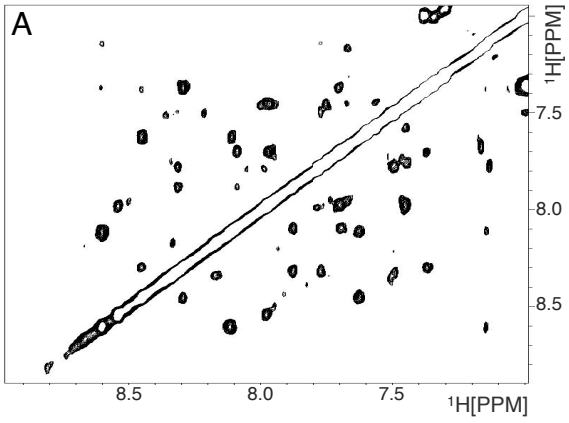
A
8.5
8.0
7.5
^{1}H[PPM]
7.5
8.0
8.5

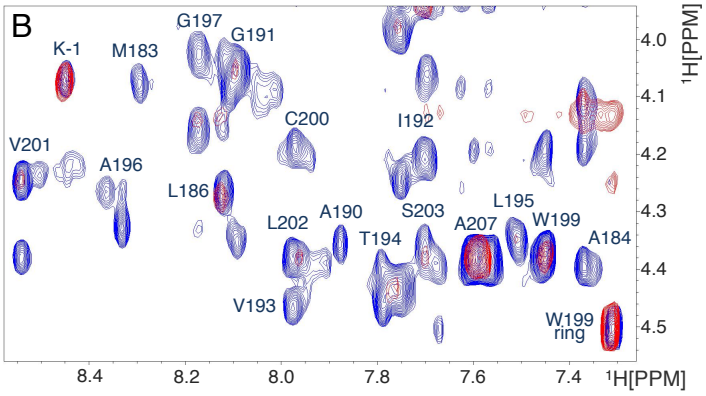
B
K-1
M183
G197
G191
C200
I192
V201
A196
L186
L202
A190
T194
S203
A207
L195
W199
A184
V193
W199
ring
8.4
8.2
8.0
7.8
7.6
7.4
^{1}H[PPM]
4.0
4.1
4.2
4.3
4.4
4.5
^{1}H[PPM]

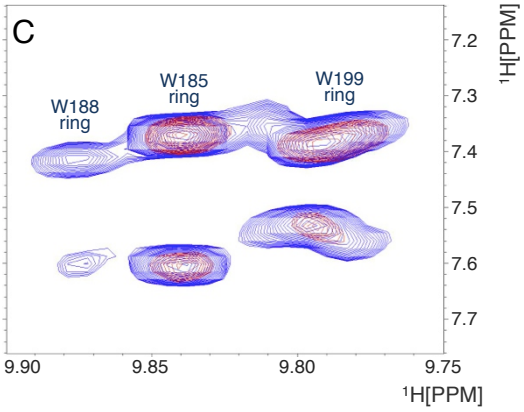
C
W188
ring
W185
ring
W199
ring
9.90
9.85
9.80
9.75
^{1}H[PPM]
7.2
7.3
7.4
7.5
7.6
7.7
^{1}H[PPM]

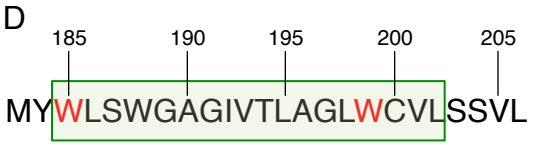
D
185
190
195
200
205
MYWLSWGAGIVTLAGLWCVLSSVL

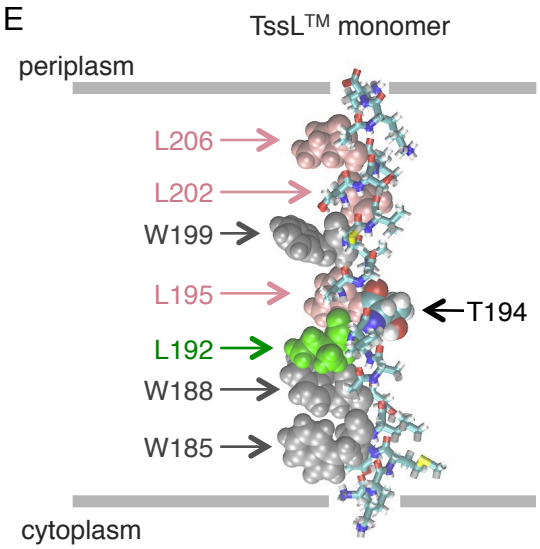
E
TssL^{TM} monomer
periplasm
L206
L202
W199
L195
T194
L192
W188
W185
cytoplasm

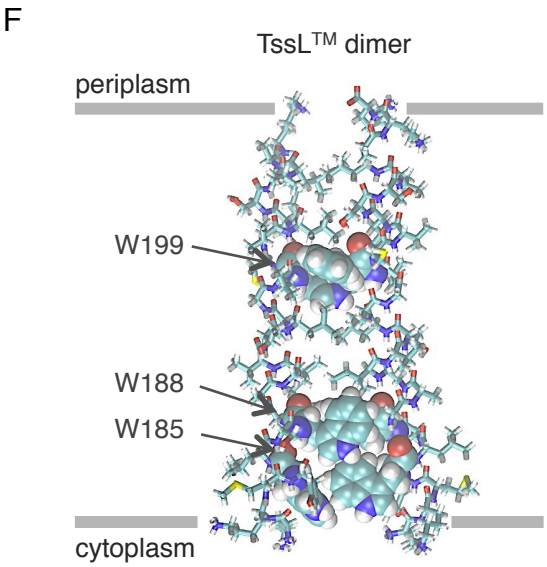
F
TssL^{TM} dimer
periplasm
W199
W188
W185
cytoplasm

Figure 5

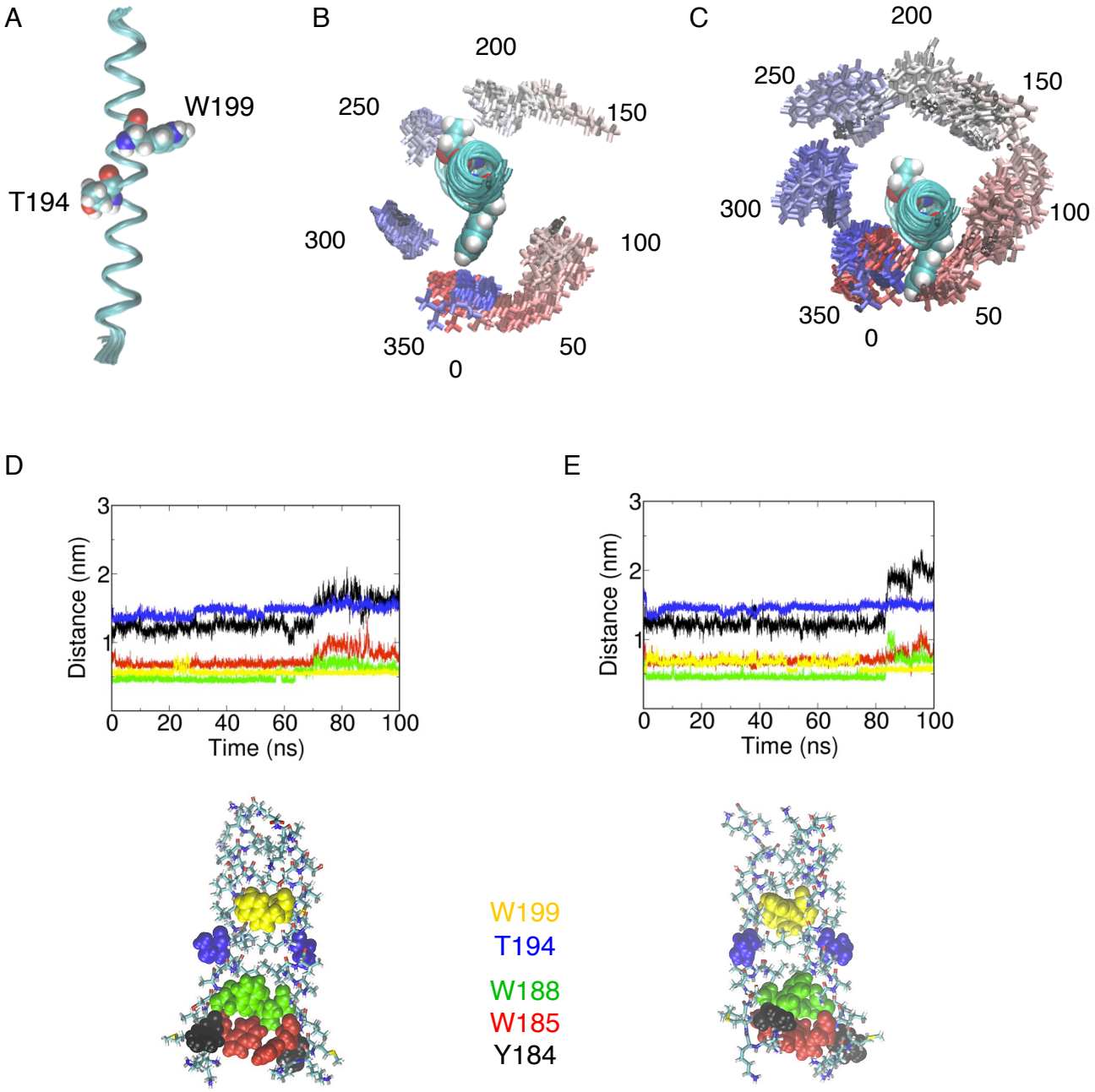
A
W199
T194
B
200
250
150
300
100
350
50
0
C
200
250
150
300
100
350
50
0
D
Distance (nm)
3
2
1
0
20
40
60
80
100
Time (ns)
E
Distance (nm)
3
2
1
0
20
40
60
80
100
Time (ns)
W199
T194
W188
W185
Y184

Figure 6

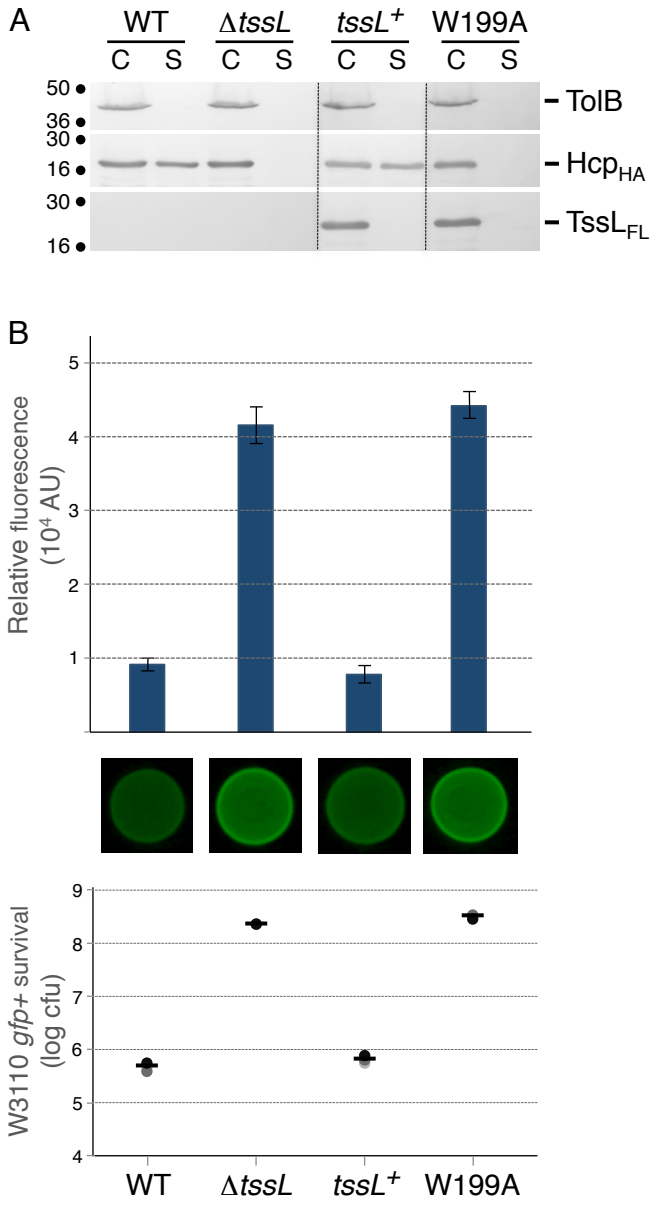
A
WT
ΔtssL
tssL+
W199A
C S C S C S C S
50
36
30
16
30
16
TolB
Hcp HA
TssL FL
B
Relative fluorescence (10⁴ AU)
5
4
3
2
1
W3110 gfp+ survival (log cfu)
9
8
7
6
5
4
WT
ΔtssL
tssL+
W199A

Figure 7

A

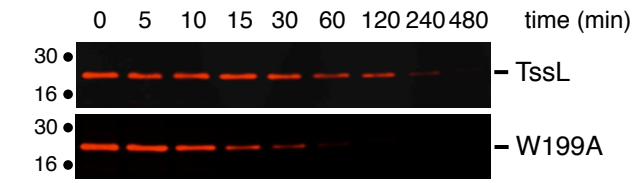
0 5 10 15 30 60 120 240 480 time (min)
30
16
TssL
30
16
W199A

B

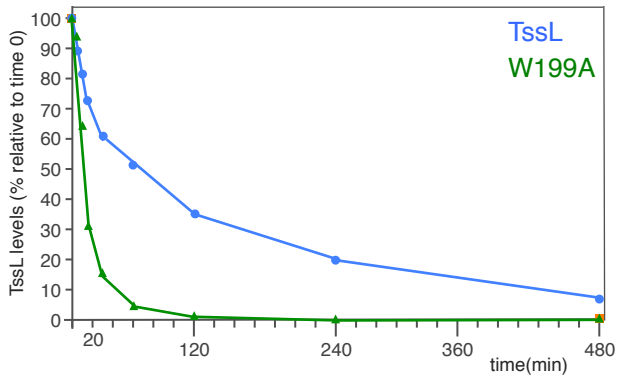
TssL levels (% relative to time 0)
100
90
80
70
60
50
40
30
20
10
0
TssL
W199A
20
120
240
360
480
time(min)

C

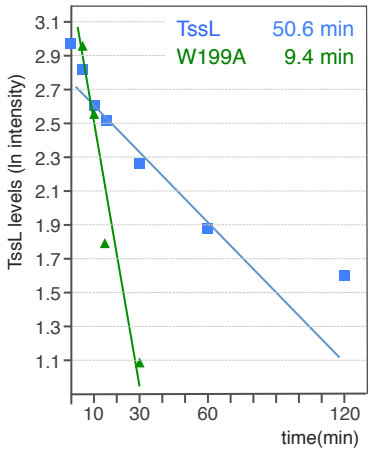
TssL levels (ln intensity)
3.1
2.9
2.7
2.5
2.3
2.1
1.9
1.7
1.5
1.3
1.1
TssL 50.6 min
W199A 9.4 min
10
30
60
120
time(min)

Figure 8

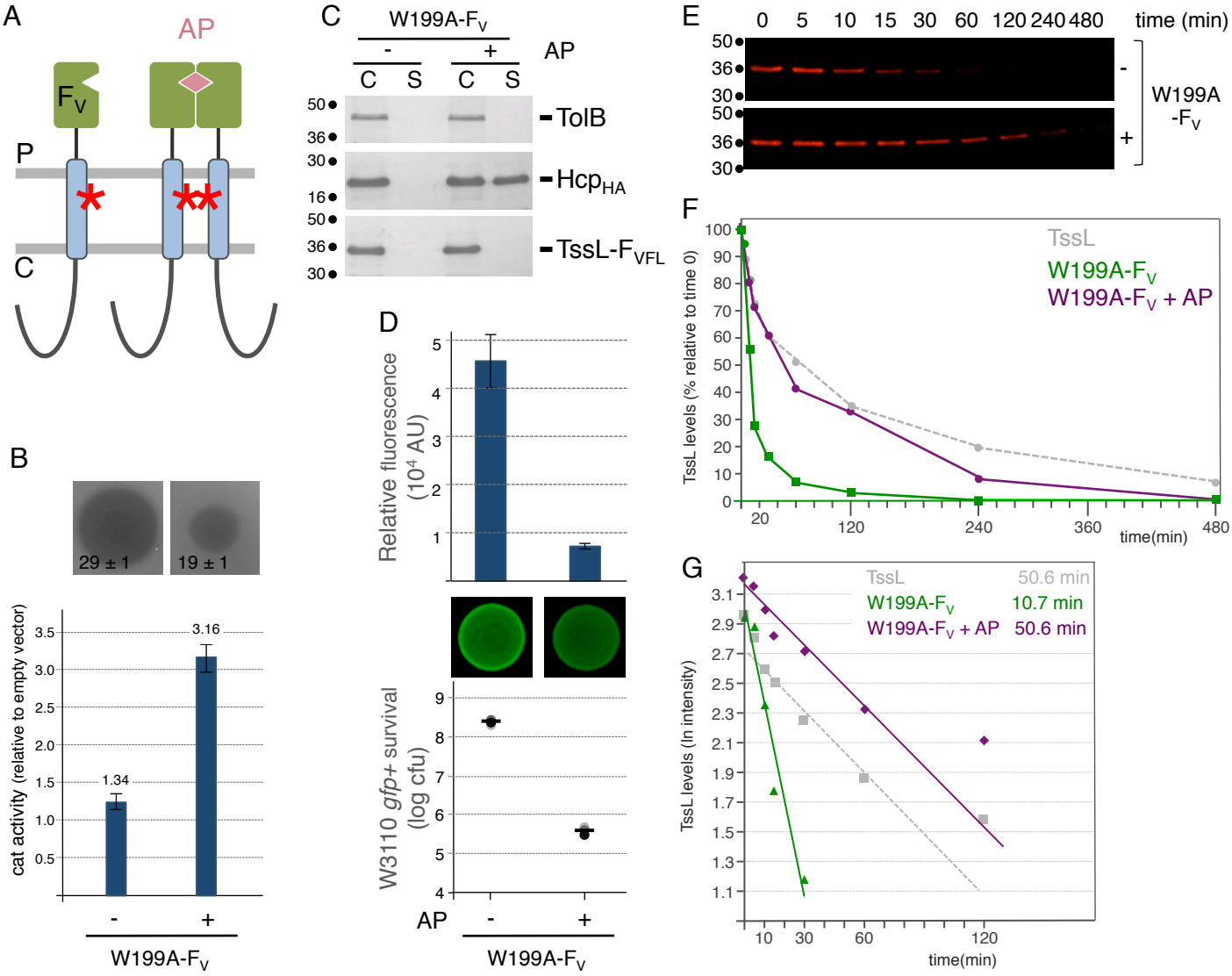
A
AP
F_V
P
C
B
29 ± 1
19 ± 1
cat activity (relative to empty vector)
3.16
1.34
W199A-F_V
C
W199A-F_V
AP
C S C S
TolB
Hcp_{HA}
TssL-F_{VFL}
D
Relative fluorescence (10^4 AU)
W3110 *gfp+* survival (log cfu)
AP
W199A-F_V
E
0 5 10 15 30 60 120 240 480 time (min)
W199A -F_V
F
TssL
W199A-F_V
W199A-F_V + AP
TssL levels (% relative to time 0)
time(min)
G
TssL 50.6 min
W199A-F_V 10.7 min
W199A-F_V + AP 50.6 min
TssL levels (ln intensity)
time(min)

Figure 9

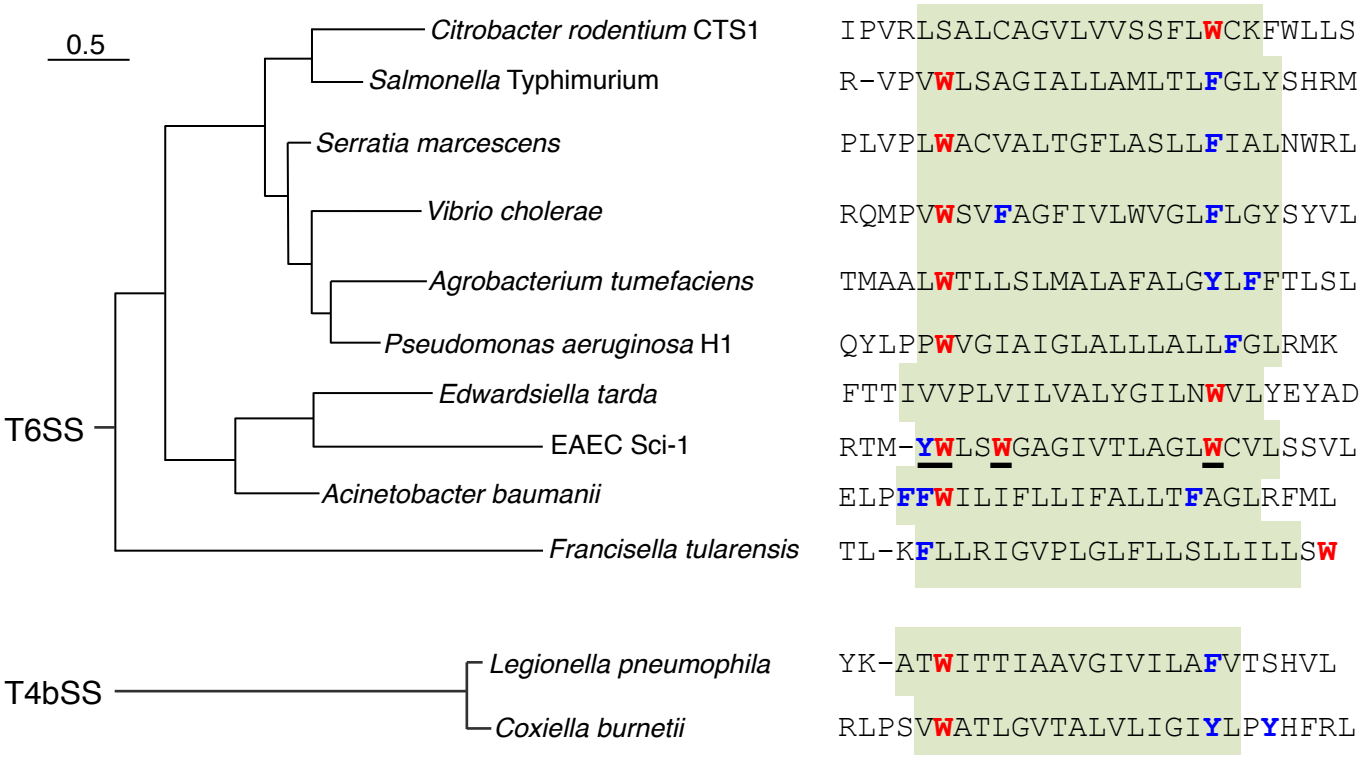
0.5
Citrobacter rodentium CTS1
Salmonella Typhimurium
Serratia marcescens
Vibrio cholerae
Agrobacterium tumefaciens
Pseudomonas aeruginosa H1
Edwardsiella tarda
EAEC Sci-1
Acinetobacter baumanii
Francisella tularensis
T6SS
T4bSS
Legionella pneumophila
Coxiella burnetii
IPVRLSALCAGVLVVSSFLWCKFWLLS
R-VPVWLSAGIALLAMLTLFGLYSHRM
PLVPLWACVALTGFLASLLFIALNWRL
RQMPVWSVFAGFIVLWVGLFLGYSYVL
TMAALWTLLSLMALAFALGYLFFTLSL
QYLPPWVGIAIGLALLLALLFGLRMK
FTTIVVPLVILVALYGILNWVLYEYAD
RTM-YWLSWGAGIVTLAGLWCVLSSVL
ELPFFWILIFLLIFALLTFAGLRFML
TL-KFLLRIGVPLGLFLLSLLILLSW
YK-ATWITTIAAVGIVILAFVTSHVL
RLPSVWATLGVTALVLIGIYLPYHFRL

Figure 10

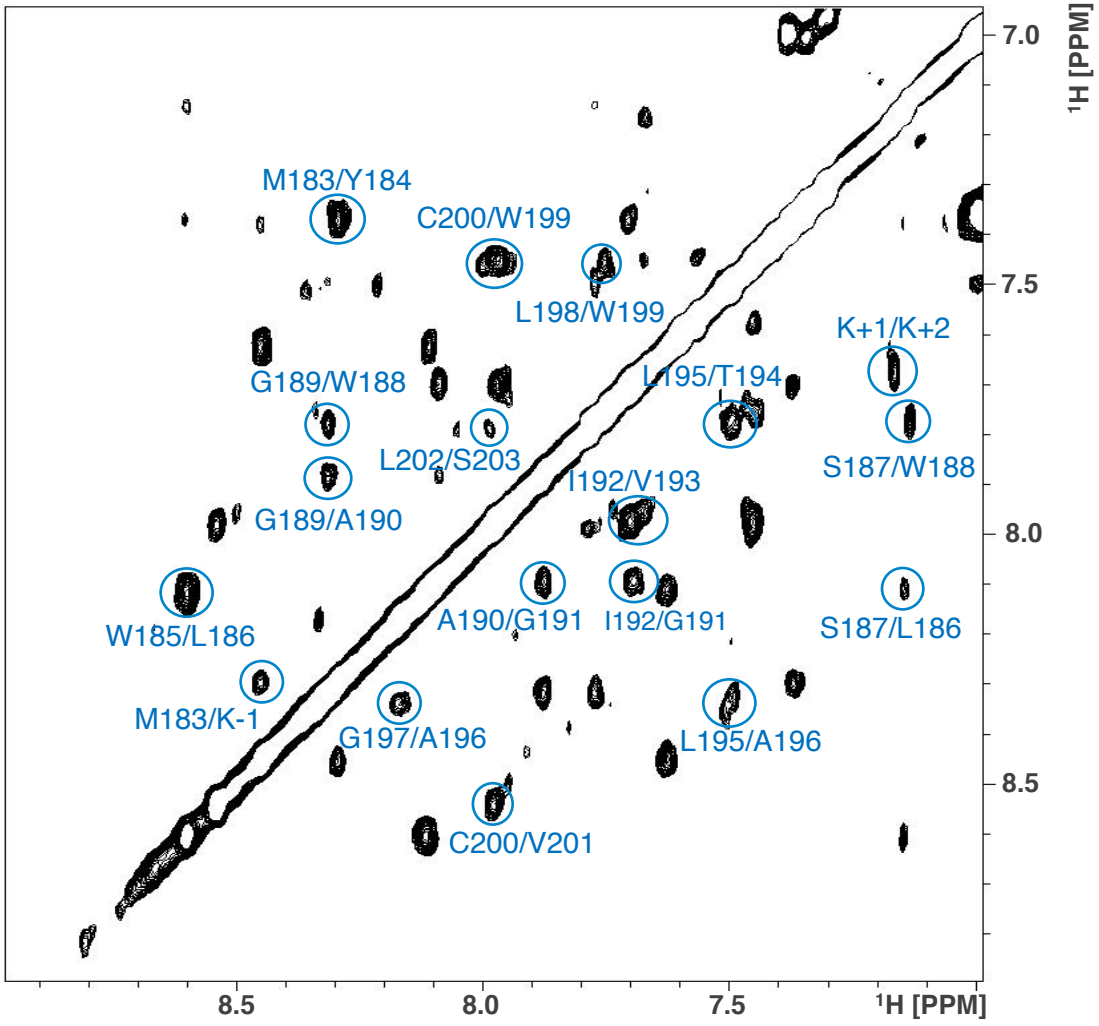
M183/Y184
C200/W199
L198/W199
K+1/K+2
G189/W188
L195/T194
L202/S203
S187/W188
I192/V193
G189/A190
W185/L186
A190/G191
I192/G191
S187/L186
M183/K-1
G197/A196
L195/A196
C200/V201
7.0
7.5
8.0
8.5
8.5
8.0
7.5
¹H [PPM]
¹H [PPM]

Figure S1

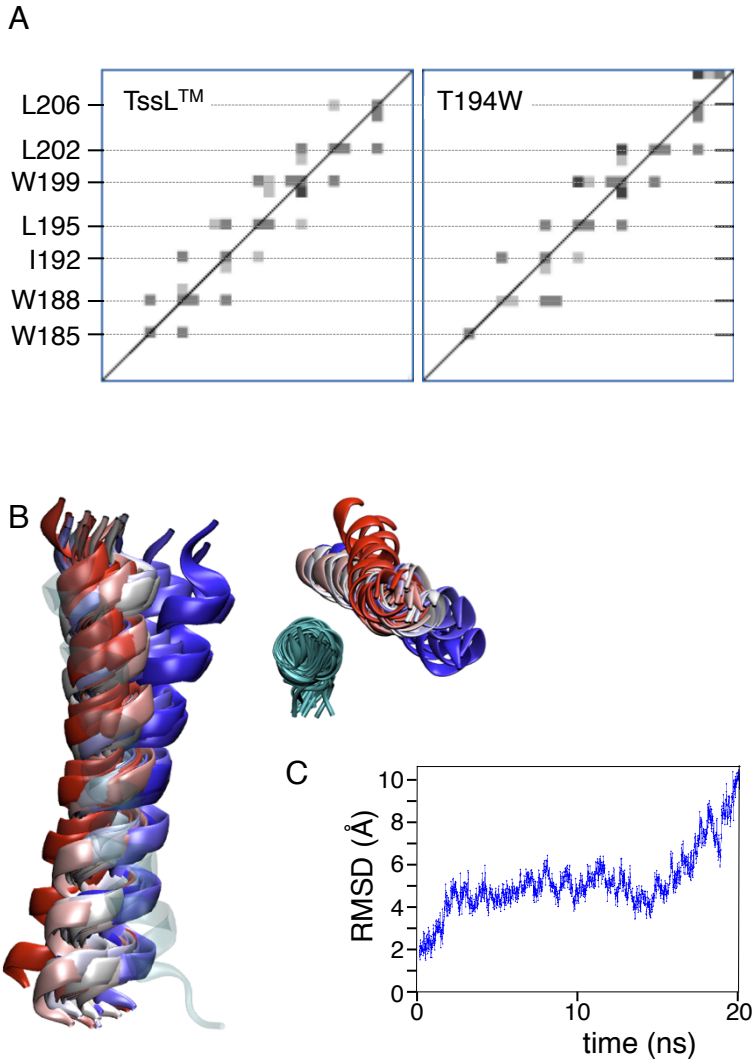
A
L206
L202
W199
L195
I192
W188
W185
TssL™
T194W
B
C
RMSD (Å)
0
2
4
6
8
10
0
10
20
time (ns)

Figure S2

Table S1. Sequential ^{1}H assignment of the TssL^{TM} peptide (residues 183-207) at 300K and pH4.5

Residue	H_N	Ha	Hb	Others
Lys-2	7.62	3.70		Hg 1.03; 0.87; He 2.13
Lys-1	8.44	3.85		Hd 1.62; Hg 1.44;0.85
Met183	8.30	3.57	3.38; 1.60	
Tyr184	7.36	4.50	3.96; 4.18	Hd 7.49; 7.00 He 7.33; 6.90
Trp185	8.60	4.48	3.34; 3.3	Hd 7.14 He 9.84; 7.81 Hh 6.98 Hz 7.37; 6.80
Leu186	8.11	4.04	1.77; 1.67	Hg 1.52 Hd 0.90; 0.80
Ser187	7.14	4.10	3.85	
Trp188	7.78	4.37	3.12; 3.29	Hd 7.18 He 9.87; 7.48 Hh 6.99 Hz 7.37; 6.80
Gly189	8.32	3.64		
Ala190	7.88	4.13	1.33	
Gly191	8.11	3.85		
Ile192	7.71	3.99	1.75	Hg 1.59; 1.34; Hd 0.64; 0.79
Val193	7.97	4.23	2.2	Hg 1.76
Thr194	7.78	4.16		Hg 1.42
Leu195	7.50	4.09	2.04	Hd 0.89; Hg 1.35
Ala196	8.33	4.10	1.40	
Gly197	8.17	3.75	3.62	
Leu198	7.70	4.13		Hd 0.98;0.82; Hg 2.13
Trp199	7.45	4.18	4.02	Hd 7.16; He 9.79;7.46; Hh 6.97; Hz 7.31;6.63
Cys200	7.99	3.98	2.18; 1.73	
Val201	8.52	4.1	1.64	Hg 1.31
Leu202	7.98	4.15	1.81; 1.60	Hg 1.31
Ser203	7.70	4.13	3.70	
Ser204	8.10	3.85	3.08; 3.00	
Val205	8.21	3.75		Hg 1.6
Leu206	8.29	3.86	1.85; 1.61	Hg 1.38
Ala207	7.69	4.13	0.98	
Lys+1	7.67	4.26	1.69	Hd 0.98; He 2.12
Lys+2	7.16	4.67	1.60	He 2.89

Supplementary Table S2. Strains, plasmids and oligonucleotides used in this study.

Strains

Strains	Description and genotype	Source
E. coli K-12		
DH5α	F-, Δ(*argF-lac*)U169, *phoA*, *supE44*, Δ(lacZ)M15, *relA*, *endA*, *thi*, *hsdR*	New England Biolabs
W3110	F-, lambda- IN(*rrnD-rrnE*)1 *rph*-1	Laboratory collection
NT326	F-, Δ(*argF-lac*)U169, *rpsL*, *relA*, *rbsR*, *flbB*, *ptsF*,*thi*, *deoC*, Δ*malE444*, *recA*	[68]
Enteroaggregative *E. coli*		
17-2	WT enteroaggregative *Escherichia coli*	Arlette Darfeuille-Michaud
17-2Δ*tssL*	17-2 deleted of the *tssL* gene of the *sci1* T6SS gene cluster	[20]

Plasmids

Vectors	Description	Source
Expression vectors		
pASK-IBA37	cloning vector, P*tet*, Amp^R	IBA Technology
pASK-IBA37-$TssL_{FL}$	*sci1 tssL* cloned into pASK-IBA37, C-terminal FLAG epitope	[25]
pASK-IBA37-$TssL_C$	Cytoplasmic domain (residues 1-183) of *sci1 tssL* cloned into pASK-IBA37, N-terminal FLAG epitope	[25]

pASK-IBA37-TssL$_{FL}$-T194W	Thr194 to Trp into pASK-IBA37-TssL$_{FL}$	This study
pASK-IBA37-TssL$_{FL}$-W199A	Trp199 to Ala into pASK-IBA37-TssL$_{FL}$	This study
pASK-IBA37-TssL$_{FL}$-W199A-FK	FK506 binding protein fused to TssL into pASK-IBA37-TssL$_{FL}$	This study
pOK-HcpHA	*sci1 hcp* cloned into pOK12, C-terminal HA epitope	[20]
pUA66-*rrnb*	*P$_{rrnB}$ ::gfpmut2* transcriptional fusion in pUA66, Kan^{R}	[71]

Vectors for TOXCAT assay

pcckan	ToxR-dependent expression of *cat*	[33]
pccGpA	pcckan plasmid with glycophorin A TMH inserted between ToxR and MBP	[33]
pccGpG83I	Gly83 to Ile into pccGpA	[33]
pcc-TssL-TM	pcckan plasmid with TssL TMH (residues 174-217) inserted between ToxR and MBP	This study
pcc-TssL-LALA	Leu-195 and Leu-198 to Ala into pcc-TssL-TM	This study
pcc-TssL-M183W	Met-183 to Trp into pcc-TssL-TM	This study
pcc-TssL-Y184W	Tyr-183 to Trp into pcc-TssL-TM	This study
pcc-TssL-W185A	Trp-185 to Ala into pcc-TssL-TM	This study
pcc-TssL-L186W	Leu-186 to Trp into pcc-TssL-TM	This study
pcc-TssL-S187W	Ser-187 to Trp into pcc-TssL-TM	This study
pcc-TssL-W188A	Trp-188 to Ala into pcc-TssL-TM	This study
pcc-TssL-G189W	Gly-189 to Trp into pcc-TssL-TM	This study
pcc-TssL-A190W	Ala-190 to Trp into pcc-TssL-TM	This study
pcc-TssL-G191W	Gly-191 to Trp into pcc-TssL-TM	This study
pcc-TssL-I192W	Ile-192 to Trp into pcc-TssL-TM	This study
pcc-TssL-V193W	Val-193 to Trp into pcc-TssL-TM	This study
pcc-TssL-T194W	Thr-194 to Trp into pcc-TssL-TM	This study
pcc-TssL-L195W	Leu-195 to Trp into pcc-TssL-TM	This study
pcc-TssL-A196W	Ala-196 to Trp into pcc-TssL-TM	This study
pcc-TssL-G197W	Gly-197 to Trp into pcc-TssL-TM	This study
pcc-TssL-L198W	Leu-198 to Trp into pcc-TssL-TM	This study
pcc-TssL-W199A	Trp-199 to Ala into pcc-TssL-TM	This study
pcc-TssL-C200W	Cys-200 to Trp into pcc-TssL-TM	This study

pcc-TssL-V201W	Val-201 to Trp into pcc-TssL-TM	This study
pcc-TssL-L202W	Leu-202 to Trp into pcc-TssL-TM	This study
pcc-TssL-S203W	Ser-203 to Trp into pcc-TssL-TM	This study
pcc-TssL-S204W	Ser-204 to Trp into pcc-TssL-TM	This study
pcc-TssL-V205W	Val-205 to Trp into pcc-TssL-TM	This study
pcc-TssL-L206W	Leu-206 to Trp into pcc-TssL-TM	This study
pcc-TssL-W199A-FK	FK506 binding protein fused to TssL-TM into pcc-TssL-W199	This study

Oligonucleotides

Name	**Destination**	**Sequence (5' → 3')**
For plasmid construction		
5-TssLTM-NheI	insertion of TssL-TM into pcckan	GGTGGTGGTGCGTGCTAGCGCACCGGGTTACCGTG
3-TssLTM-BamHI	insertion of TssL-TM into pcckan	CGTACGTGCATGGTTAGGATCCCTCCCTGCCCGGTAAGCC
5-pcckn-L-TM-FKBP	FK506 binding protein fused to TssL-TM	CAGGTGGCACGGCTTACCGGGCAGGGAGGGCTCGAGATGGCTTCTAGAGGAGTGCAGGTG
3-pcckn-L-TM-FKBP	FK506 binding protein fused to TssL-TM	GTTTAAAGCTGGATTGGCTTGGGTTGATCAGGATTCATTCCAGTTTTAGAACCTTCACATCG
5-IBA-TssL-LFKBP	FK506 binding protein fused to TssL	CAGGTGGCACGGCTTACCGGGCAGGGACTCGAGATGGCTTCTAGAGGAGTGCAGG
3-IBA-TssL-FKBP	FK506 binding protein fused to TssL	GATGGTGATGCGATCCTCTGCTAGCTCATTCCAGTTTTAGAACCTTCACATCGAAG
For site directed mutagenesis		
5-TssL-L195A-L198A	Leu195 to Ala and Leu198 to Ala	GGGGCGGGTATTGTGACGGCGGCTGGTGCCTGGTGTGTGCTTTCTTC

3-TssL-L195A-L198A	Leu195 to Ala and Leu198 to Ala	GAAGAAAGCACACACCAGGCACCAGCCGCCGTCACAA TACCCGCCCC
5-A-M183W	Met183 to Trp	GTTACCGTGCTGGCAGAACGTGGTACTGGTTGTCATGG GGG
5-A-Y184W	Tyr183 to Trp	GTTACCGTGCTGGCAGAACGATGTGGTGGTTGTCAT GGGGGGCG
5-A-W185A	Trp185 to Ala	GTTACCGTGCTGGCAGAACGATGTACGCGTTGTCATG GGGGGCGGG
5-A-L186W	Leu186 to Trp	GTTACCGTGCTGGCAGAACGATGTACTGGTGGTCAT GGGGGGCGGGTAT
5-A-S187W	Ser187 to Trp	GTTACCGTGCTGGCAGAACGATGTACTGGTTGTGGTG GGGGGCGGGTATTGTG
3-A-M183-S187		TCTGCCAGCACGGTAACCCGGTGCACGCAC
5-B-W188A	Trp188 to Ala	GAACGATGTACTGGTTGTCAGCGGGGGCGGGTATTGT GAC
5-B-G189W	Gly189 to Trp	GAACGATGTACTGGTTGTCATGGTGGGCGGGTATTGTG ACG
5-B-A190W	Ala190 to Trp	GAACGATGTACTGGTTGTCATGGGGGTGGGGTATTGT GACGCT
5-B-G191W	Gly191 to Trp	GAACGATGTACTGGTTGTCATGGGGGGCGTGGATTGT GACGCTGGC
5-B-I192W	Ile192 to Trp	GAACGATGTACTGGTTGTCATGGGGGGCGGGTTGGGT GACGCTGGCTGG
3-B-W188-I192		CAACCAGTACATCGTTCTGCCAGCACGGTA
5-C-V193W	Val193 to Trp	TGTCATGGGGGGCGGGTATTTGGACGCTGGCTGGTCTC TGG
5-C-T194W	Thr194 to Trp	TGTCATGGGGGGCGGGTATTGTGTGGCTGGCTGGTCTC TGGTG
5-C-L195W	Leu195 to Trp	TGTCATGGGGGGCGGGTATTGTGACGTGGGCTGGTCTC TGGTGTG
5-C-A196W	Ala196 to Trp	TGTCATGGGGGGCGGGTATTGTGACGCTGTGGGGTCTC TGGTGTGTG

5-C-G197W	Gly197 to Trp	TGTCATGGGGGGCGGGTATTGTGACGCTGGCTTGGCTCTGGTGTGTGCTT
3-C-V193-G197		ACCCGCCCCCCATGACAACCAGTACATCGT
5-D-L198W	Leu198 to Trp	GTATTGTGACGCTGGCTGGTTGGTGGTGTGTGCTTTCTTCT
5-D-W199A	Trp199 to Ala	GTATTGTGACGCTGGCTGGTCTCGCGTGTGTGCTTTCTTCTGTG
5-D-C200W	Cys200 to Trp	GTATTGTGACGCTGGCTGGTCTCTGGTGGGTGCTTTCTTCTGTGCT
5-D-V201W	Val201 to Trp	GTATTGTGACGCTGGCTGGTCTCTGGTGTTGGCTTTCTTCTGTGCTTGC
5-D-L202W	Leu202 to Trp	GTATTGTGACGCTGGCTGGTCTCTGGTGTGTGTGGTCTTCTGTGCTTGCAG
3-D-L198-L202		AGCCAGCGTCACAATACCCGCCCCCCATGA
5-E-S203W	Ser203 to Trp	CTGGTCTCTGGTGTGTGCTTTGGTCTGTGCTTGCAGACCAG
5-E-S204W	Ser204 to Trp	CTGGTCTCTGGTGTGTGCTTTCTTGGGTGCTTGCAGACCAGGTG
5-E-V205W	Val205 to Trp	CTGGTCTCTGGTGTGTGCTTTCTTCTTGGCTTGCAGACCAGGTGGCA
5-E-L206W	Leu206 to Trp	CTGGTCTCTGGTGTGTGCTTTCTTCTGTGTGGGCAGACCAGGTGGCACG
3-E-S203-L206		CACACACCAGAGACCAGCCAGCGTCACAAT